



Swansea University
Prifysgol Abertawe



Cronfa - Swansea University Open Access Repository

This is an author produced version of a paper published in:

Marine Geology

Cronfa URL for this paper:

<http://cronfa.swan.ac.uk/Record/cronfa45567>

Paper:

Yin, Y., Karunaratna, H. & Reeve, D. (2018). Numerical modelling of hydrodynamic and morphodynamic response of a meso-tidal estuary inlet to the impacts of global climate variabilities. *Marine Geology*

<http://dx.doi.org/10.1016/j.margeo.2018.11.005>

This item is brought to you by Swansea University. Any person downloading material is agreeing to abide by the terms of the repository licence. Copies of full text items may be used or reproduced in any format or medium, without prior permission for personal research or study, educational or non-commercial purposes only. The copyright for any work remains with the original author unless otherwise specified. The full-text must not be sold in any format or medium without the formal permission of the copyright holder.

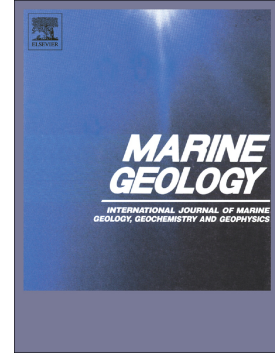
Permission for multiple reproductions should be obtained from the original author.

Authors are personally responsible for adhering to copyright and publisher restrictions when uploading content to the repository.

<http://www.swansea.ac.uk/library/researchsupport/ris-support/>

Accepted Manuscript

Numerical modelling of hydrodynamic and morphodynamic response of a meso-tidal estuary inlet to the impacts of global climate variabilities



Yunzhu Yin, Harshinie Karunaratna, Dominic E. Reeve

PII: S0025-3227(18)30084-7
DOI: <https://doi.org/10.1016/j.margeo.2018.11.005>
Reference: MARGO 5875
To appear in: *Marine Geology*
Received date: 22 March 2018
Revised date: 29 October 2018
Accepted date: 6 November 2018

Please cite this article as: Yunzhu Yin, Harshinie Karunaratna, Dominic E. Reeve , Numerical modelling of hydrodynamic and morphodynamic response of a meso-tidal estuary inlet to the impacts of global climate variabilities. *Margo* (2018), <https://doi.org/10.1016/j.margeo.2018.11.005>

This is a PDF file of an unedited manuscript that has been accepted for publication. As a service to our customers we are providing this early version of the manuscript. The manuscript will undergo copyediting, typesetting, and review of the resulting proof before it is published in its final form. Please note that during the production process errors may be discovered which could affect the content, and all legal disclaimers that apply to the journal pertain.

Numerical modelling of hydrodynamic and morphodynamic response of a meso-tidal estuary inlet to the impacts of global climate variabilities

Yunzhu Yin, Harshinie Karunaratna, Dominic E. Reeve

Energy and Environment Research Group, Zienkiewicz Centre
for Computational Engineering, College of Engineering, Bay
Campus, Swansea University, Fabian Way, Swansea, SA1 8EN,
UK

Corresponding author: Harshinie Karunaratna,
h.u.karunaratna@swansea.ac.uk

Abstract

Tidal inlets, a common feature along coastlines globally, can be significantly affected by the impacts of global climate variabilities. Computational models provide the best opportunity to assess future changes to the dynamics of inlet systems. In this paper, the morphodynamic response of a gravel-dominated meso-tidal estuary inlet to Sea Level Rise (SLR) is discussed based on three future SLR scenarios. It uses a process-based computational coastal area model. The study's

test site is the meso-tidal Deben Estuary inlet in the UK; it is very morphodynamically active and has a unique sediment environment, is used as the test site of this study. The modelling results reveal that the morphological response of Deben inlet is sensitive to the SLR scenario. Rising sea levels give rise to increased hydrodynamic and morphodynamic activities at and around the inlet. The ebb delta, which is a prominent morphodynamic feature of this inlet, shows greater instability as a result of increased sea levels. It is possible that the inlet may deviate significantly from its current morphodynamic regime in the future as a result of the changes imposed by higher sea levels.

Keywords: Deben Estuary; inlet; meso-tidal; morphodynamics; computational modelling; sea level rise; climate change.

1. Introduction

An estuary's inlet is the river entrance: it plays an important role in the evolution of the estuary. Morphodynamics of tidal inlets are usually controlled by the interaction of tides, waves and river flows along with sediment properties and availability (Finley, 1978; Boothroyd, 1985; Douglas et al., 2001). The inlet evolution is not only related to the intensive

hydrodynamic conditions such as storm surges or extreme wave conditions in the short term (Anthony et al., 2004; Dissanayake et al., 2014). It is also influenced by mean sea level, tidal fluctuation, and wave propagation over a long period of time (Zacharioudaki and Reeve, 2011). As a result, any changes to mean sea level and incident wave climate due to future climate variabilities may have significant implications on future morphodynamics behaviour of the inlet.

SLR is one of the most significant impacts of global climate variabilities. The Inter-Governmental Panel on Climate Change (IPCC) has projected global sea levels by the end of 21st century using several green-house gas emission scenarios (Houghton et al., 2001). It is reported that the rate of global SLR during the 21st century is between 1.0mm/year to 2.0mm/year with a central value of 1.5mm/year (Houghton et al., 2001). It has been estimated that, on average, the mean sea level around UK will increase by 20cm according to the lowest green-house gas emission scenario; however, according to the highest emission scenario, it may be as high as 80cm by the end of this century (Lowe et al., 2009; Hulme et al., 2002).

Therefore, a discussion of the response to increasing sea levels should be an integral part of any investigation into future morphodynamic behaviour of estuarine inlets.

While there is a vast amount of literature on climate change impacts on open coasts (see Ranasinghe, 2016 for a comprehensive review of previous literature), studies on climate change impacts on estuaries are limited. Van Goor et al. (2003) applied ASMITA, a reduced-complexity morphodynamic model, to two schematised estuaries in dynamic equilibrium. They investigated the impacts of SLR on the morphodynamic equilibrium of tidal inlets. They found that with SLR, an estuary can evolve into a new equilibrium state if a sufficient supply of sediment is maintained. Otherwise, the system will deviate from its original equilibrium state and will degenerate. Karunarathna and Reeve (2008) and Reeve and Karunarathna (2009) used a model based on Boolean Algebra to investigate morphodynamic responses of estuaries to SLR. They found that sediment availability plays a crucial role when an estuary adjusts to future sea levels. Karunarathna et al. (2008) combined a reduced-physics modelling approach with historic bathymetry data to investigate long-term evolution of Humber Estuary in the UK. Although the model was able to capture historic long-term morphodynamic trends of the estuary, assumptions that should be made when extrapolating past trends to future incurred some limitations when investigating future climate change impacts.

Process-based models provide the best opportunity to accurately simulating morphodynamic behaviour of estuaries. However, the application of such models over the long-period required to investigate climate change impacts has some limitations. These include the vast computational costs involved, uncertainty in future hydrodynamic boundary conditions and accumulation of errors in long-term simulations.

In recent years, some process-based modelling efforts to investigate climate change impacts on estuaries and inlets have been reported. Dissanayake et al. (2009) and Dissanayake (2011), used a schematic bathymetry and simplified representative hydrodynamic forcings to model climate change impacts on the Ameland Inlet in the Netherlands using a process-based Delft3D model (Lesser et al., 2004). They observed that if future SLR is moderate, the inlet will be able to adjust to future sea levels. However, in the event of extreme SLR, the estuary will drown. Taking future ‘snap shot’ approach, Duong et al. (2017) computationally modelled three different types of schematic sandy, micro-tidal inlets (Type 1 - stable inlet, Type 2 - permanently open, longshore migrating; Type 3 - seasonally intermittently open, spatially stable) using Delft3D. They also used schematic bathymetries and simplified hydrodynamic forcing conditions. Their modelling revealed

that all three inlet types were sensitive to climate change driven changes to the longshore transport regime rather than to SLR and have the tendency to be unstable in future and that inlet Type 2 has the tendency to move into Type 1 as a result of climate change. Duong et al. (2018) modelled the same three inlets using actual bathymetries and future hydrodynamic forcings dynamically downscaled from the IPCC Global Climate Model. Their results revealed that all three inlet types will experience significant changes to their stability but none will change their type as a result of future climate change impacts.

Most of the existing studies investigating climate change impacts on estuary systems have focused on sand-dominated systems in micro-tidal environments. However, the majority of inlet systems in the UK are either meso-tidal or macro-tidal. Furthermore, although sandy and muddy inlets are common around the world, coarse or mixed-sediment inlets can be found in many parts of the UK and worldwide. Very little is currently known about their future morphodynamic behaviour. Our motivation in this study is to investigate detailed morphodynamic behaviour of a meso-tidal, mixed-sediment estuary inlet in a changing climate, using a process-based hydrodynamic-morphodynamic model.

The Deben Estuary inlet located in the east coast of the United Kingdom (UK) will be used as the test site. The Deben Estuary inlet is a gravel-dominated sand-gravel mixed sediment system. The estuary is subjected to a meso-tidal regime while incoming wave energy conditions are classified as medium. It is unclear if its morphodynamic response to future climate variabilities in mixed sediment estuaries is similar to that of sandy systems as sediment characteristics can influence littoral transport regime over a range of timescales and cause morphodynamic change. The Deben Estuary is unique in its meso-tidal, medium wave energy hydrodynamic regime that may have led to its distinctly complex morphodynamic behaviour where the inlet delta cyclically evolves through a range of morphodynamic states over time. Furthermore, the estuary has an impressive historic bathymetry dataset which can be extremely useful for model development and validation.

Considering the limitations of applying a process-based model over a long period of time, our approach here is that taking the current bathymetry of the estuary as the initial bathymetry, we will apply global climate change induced 'future' hydrodynamic and sea level conditions as boundary conditions to explore how the estuary will behave morphodynamically under future conditions over a specified period of time. The

simulated change will then be compared to the changes induced under ‘current’ conditions over the same time period to investigate the impacts of climate change. While this will provide insight into how the estuary will change in future, the gradual adaption of the estuary to SLR will not be captured.

This paper is structured as follows: Section 2 introduces the study site. Section 3 provides the details of the model and model development. The application of the model and results are given in Section 4. The paper ends with conclusions presented in Section 5.

2. Study site

The Deben Estuary is a unique spit-enclosed estuary in the UK, which demonstrates a very complex morphodynamic behaviour (Posford Duvivier, 1999; UK Hydrographic Office (UKHO), 2000; HR Wallingford, 2002; Burningham and French, 2006).

The estuary is located in the south-east coast of the United Kingdom (UK), in Suffolk (Fig. 1). It is an important part of the Suffolk coastline and contributes to hydrodynamics and morphodynamics of the Suffolk coastal system. The intertidal

middle and upper parts of the estuary are dominated by a single meandering channel while immediately landward of the estuary mouth (inner estuary) is divided by a large intertidal shoal, Horse Sand, north of which is flood dominated and south of which is ebb dominated (Fig. 1). The main inlet (throat) of the estuary, about 180m wide, connects the inner estuary to the outer estuary where a subtidal channel and intertidal ebb shoals coexist. This channel and south-directed ebb-tidal delta have changed their courses frequently and significantly in history. The positions of the main channel at the outer estuary and the state of the ebb tidal delta have changed frequently thus changing the hydrodynamic and morphodynamic regimes continuously.

Although the Deben Estuary is tide-dominated, it is also subjected to moderately high energy waves and a complex littoral sediment transport regime (Burningham and French, 2006). The morphodynamic behaviour of the ebb-tidal delta, a key morphological feature of the estuary, is likely to be sensitive to any major changes of the external forcing of mean sea levels, waves and surges (Burningham and French, 2006).

The seabed offshore of the Estuary comprises a mixture of mud, fine sand and broken shells. The inlet and outer Deben Estuary mainly consist of a mixture of gravel and sand (HR Wallingford, 2002). Sandy gravel is found throughout the ebb-tidal delta and adjacent coastal beaches of the estuary while gravel-sized material is found in the channels (Posford Duviol, 1999; Burningham and French, 2006). Mud dominates the middle and upper reaches of the estuary. Our concern in this research is the inlet area, which is the most morphodynamically active part of the estuary.

Position of Figure 1

Suffolk coast is meso-tidal and the mean spring tidal range varies from 3.2m at Felixstowe Ferry to 3.6m at Woodbridge (Fig. 1) (UKHO, 2000). The Deben Estuary has a tidal length of about 18 km from its inlet. The tidal prism is currently about $12 \times 10^6 \text{m}^3$ (Burningham and French, 2006). The average offshore wave height is around 0.96m. The predominant wave direction is north-east where around 50% of the waves reach the Suffolk coastline from that direction. 32% of the waves comes from the south-west (HR Wallingford, 2002). Strong tidal currents contribute to alignment of the sandbanks that

exist offshore of Suffolk although waves contribute to large-scale littoral drift (HR Wallingford, 2002). However, the inner estuary does not experience significant wave propagation where only locally generated fetch-limited waves, are observed (Burningham and French, 2006).

Position of Figure 2.

Deben Estuary has been extensively monitored in the past: where the estuary's bathymetry has been measured at regular intervals. Historically, the estuary had undergone a cyclic morphodynamic behaviour where the outer estuary has moved between three distinguished morphodynamic states (Fig. 2): (A) the ebb-jet migrated to the downdrift side as a result of longshore extension of the updrift ebb-tidal shoal; (B) the updrift shoal was broken and the ebb-jet moved to a more northerly position, causing diversion of the ebb channel; (C) the ebb-jet shifted the location to further north, breaking the updrift shoal with a new channel and in-filling the void left by the ebb-jet. Based on measured bathymetries over a period of 150 years Burningham and French (2006) estimated that the duration of one such morphodynamic cycle varies between 10 to 30 years. In most recent morphodynamic cycles, the evolution of the inlet

from State 1 to State 3 lasted about 20 years while the breakdown from State 3 to State 1 took about 2 years (Burningham and French, 2006). This indicates that State 3 is likely to be the most unstable morphodynamic state of the inlet compare to the others. Historic measurements also reveal that morphology of the inner estuary where flood tidal delta divides the main channel into flood-dominated channel (north of flood tidal delta) and ebb dominated channel (south of flood tidal delta) is fairly stable.

Position of Figure 3.

3. Deben Inlet morphodynamic model

This study uses the process-based coastal area model Delft3D (Lesser et al., 2004), in which the flow model and SWAN wave model (Booij, et al., 1999) are online coupled. The flow and wave models are then linked to a sediment transport and bed-updating model. Delft3D has been extensively used for estuary morphodynamic investigations (see Dissanayake et al., 2009; Duong et al., 2017, 2018). It has proven be a successful tool in capturing estuary morphodynamic behaviours (van der Wegen

and Roelvink, 2012). As we are interested in sea bed dynamics, the depth-averaged version of Delft3D is used.

3.1. Computational model of the Deben Estuary

To optimise grid sizes, computational domain, computational time and, considering available boundary conditions, a nested modelling procedure is used to develop the computational hydrodynamic-morphodynamic model of the Deben Estuary. As shown in Fig. 4, three domains are nested. The largest domain, Domain A has an area around $3.46 \times 10^3 \text{ km}^2$ in which grid sizes vary from $3 \text{ km} \times 500 \text{ m}$ offshore to $800 \text{ m} \times 500 \text{ m}$ onshore; the medium domain, Domain B covers $1.32 \times 10^3 \text{ km}^2$. Grid sizes in Domain B vary from $720 \text{ m} \times 160 \text{ m}$ offshore to $270 \text{ m} \times 160 \text{ m}$ onshore; The smallest domain, Domain C covers an area of approximately $18 \text{ km} \times 6 \text{ km}$ and has grid resolution of approximately $220 \text{ m} \times 100 \text{ m}$ offshore and $160 \text{ m} \times 50 \text{ m}$ onshore. The hydrodynamic boundary conditions of the smallest domain in which morphodynamics were modelled (Domain C), were obtained from the larger domains. To explore the hydrodynamics and morphodynamics of the Deben inlet area in detail, further refinement of grid size in the estuary is required. To satisfy this requirement we introduced the Domain

Decomposition (DD) technique to the smallest domain

(Domain C, Fig. 6).

Position of Figure 4.

Two nested domains are used for the wave module (Domain A and Domain C) in order to reduce the computational time. The stationary 3rd generation SWAN wave model (Booij, et al., 1999) incorporated in Delft3D is used for wave simulations.

The spatial distribution of medium sediment diameter (D_{50}) in the Deben Estuary and its surroundings is shown in Fig. 5 (Posford Duvivier, 1999; HR Wallingford, 2002; Burningham and French, 2006). D_{50} values in the main channel, flood tidal delta at the inner estuary (Horse Sand) and the ebb shoal area are 42.2mm, 0.4mm and 7.0mm respectively. In all other places, D_{50} is around 5.5mm on average. Due to the scarcity of information on sediment characteristics in the estuary, a single sediment fraction for all sediment sizes is used in the model.

Position of Figure 5.

Historic bathymetries of Deben Estuary have been derived from digitised trinity house surveys and UKHO Admiralty charts, supported by information from aerial photography, maps and Lidar surveys (Burningham and French, 2006). There are 13 bathymetry datasets in this estuary, from 1991 to 2013.

3.2. Model validation

The model validation purposes in this study, bathymetry of year 2002 is selected as the initial bathymetry of the model because of the availability of wave and tidal data in 2002.

Three sets of historic wave measurements were used for model validation: (i) Measured wave data at ‘West Gabbard’ wave rider (position: $51^{\circ}58'46''\text{N}$, $01^{\circ}26'47''\text{E}$) provided by the Centre for Environment, Fisheries and Aquaculture Science of the UK (CEFAS) at the offshore. (ii) Wave measurements collected by ‘Felixstowe Wave Rider’ in the year of 2012 (FW: $51^{\circ}56'18''\text{N}$, $01^{\circ}23'37.8''\text{E}$) (Fig. 4), which was located around 6km southeast from Deben Estuary. (iii) Hindcast wave data available from WaveWatch III at the position in Domain B (Hindcast Felixstowe Wave Rider, ‘FW_H’, $51^{\circ}53'1.68''\text{N}$,

01°26'18.96"E) (Fig. 4). The first data set is treated as the boundary condition for the wave model while the last two are used to validate the wave model. Tidal measurements are available at two locations within the Domain C (Fig. 6): (i) Felixstowe Tide gauge (FT, position: 51°57'24.3"N, 1°20'54.2"E) whose data was collected from British Oceanographic Data Centre (BODC) and (ii) Bawdsey tide gauge (BT, position: 52°00'0.32"N, 1°25'58.8"E) which was operated by the International Hydrographic Organization (IHO). The FT gauge is located about 4.5km to the south of the Deben Estuary and the BT gauge is at the depth of 4.5m and 3.5km from the inlet, shown in Fig. 6. All tide data was used to validate the hydrodynamic model. Mean Absolute Error (MAE) and Root Mean Square Error (RMSE) are used to compare measured and simulated waves and hydrodynamics within the model domains. Historic annual bathymetry data (Burningham and French, 2006) was used to validate the morphodynamic model. The Brier Skill Score (BSS) was used for the comparison of measured and simulated morphodynamic change of the Deben Estuary (Murphy and Epstein, 1989; Van Rijn et al., 2003).

Position of Figure 6.

3.2.1. Hydrodynamic validation

The tidal boundary conditions for the largest domain were taken from the TPXO7.2 Global Inverse Tidal model (from Oregon State University, <http://volkov.oce.orst.edu/tides/TPXO7.2.html>). The 13 tidal components were selected for the computation. The larger computational domains provide tidal boundary conditions for the smaller domains.

Position of Figure 7.

The three most important model calibration parameters that impact hydrodynamic results are bed roughness (described by Chèzy coefficient C), horizontal eddy viscosity coefficient (ν_h) and the threshold depth for drying and flooding ($Dryflc$). The model is calibrated against a set of three values of each parameter and the ones that gave best comparisons (smallest RMSE and MAE) with measured data were selected.

Following the calibration process, $C = 65 \text{ m}^{1/2}/\text{s}$, $\nu_h = 1 \text{ m}^2/\text{s}$ and $Dryflc = 0.1$, were used in all numerical simulations.

Once the model parameters were calibrated, the model was validated against measured data. The comparison between modelled and measured water elevations at two tide gauges FT and BT between 7th to 13th of September 2002 are shown in Fig.

6. The results show that the model captured water surface variations and tidal phase at both locations accurately. The slight discrepancy between measured and modelled tidal peaks at FT site may be attributed to the shallow water effects at FT (mean water depth is around 4.5m with tidal range varying between 1.4m to 3.8m).

The MAE and RMSE values between measured and modelled water elevations at station FT are 0.24m and 0.31m while the values at station BT are 0.06m and 0.08m respectively. This represents a 6% and 2% difference between measured and modelled tidal amplitudes at FT and BT respectively. Therefore, it is reassured that the model is able to accurately reproduce tidal hydrodynamics.

3.2.2. *Wave model validation*

Before validation of the wave model, important model parameters were calibrated. Through a series of sensitivity test, it was found that JONSWAP spectrum gives the best representation of wave conditions at the test site. The bottom friction factor for the wave model was determined based on a series of tests conducted using different values. It was found that the Hasselmann et al. (1973) model with friction factor of 0.067 gave better comparisons with measured wave data than the Collins (1972) drag law model and the Madsen et al. (1998) eddy-viscosity model.

The wave model validation was carried out using hindcast wave data at ‘Felixstowe Wave Rider’ (FW_H), located in Domain B (Fig. 4). The significant wave height (H_s) is used for model validation (Dickson et al., 2007). The boundary conditions of the wave model are taken from CEFAS WAVENET wave measurements at ‘West Gabbard’ wave rider (Fig. 4).

Position of Figure 8.

Comparisons of measured and simulated wave data at FW_H site is shown in Fig. 8. It can be seen that the model correctly reproduced H_s values at FW_H location. Small discrepancies between measured and modelled data can be attributed to measurement errors, slight difference in wave measurement location and the closest grid point where simulated data was extracted and also due to the fact that local wind effects are not considered in the model.

It is important to compare modelled and measured wave data at Domain C, where most morphodynamic changes would take place. However, measured data at FW, which is located in the Domain C is available only from year 2012 onwards, which is outside the primary simulation time period (year 2002).

Therefore, an additional validation using 2012 wave data (the boundary conditions of year 2012 are taken from the 'West Gabbard' wave rider) is carried out over a period of two months in 2012: the 2012 measured bathymetry is taken as the initial bathymetry. The results and the comparisons of measured and modelled H_s at both sites (FW and FW_H) are shown in Fig. 9. The model satisfactorily reproduced H_s values in Domain C. At FW, both the higher H_s values and lower H_s values were accurately reproduced by the model.

Position of Figure 9.

The MAE and RMSE values between measured and modelled results at FW site are 0.14m and 0.19m respectively and at FW_H are 0.27m and 0.37m respectively. The slightly higher errors at FW_H may be attributed to two aspects: i) the numerical techniques and formulations for wind input and the whitecapping in SWAN model is different to WAVEWATCH III (from where the hindcast FW_H were determined); and ii) the time interval between consecutive model outputs of SWAN model is every 6 hours, which may have led to missing some peak wave heights.

3.2.3. Morphodynamic validation

Morphodynamic validation includes two parts: (i) sensitivity analysis on Morphodynamic acceleration factor (Morfac) (Lesser et al., 2004; Roelvink, 2006) to be used in this study to accelerate morphodynamic computations; (ii) validation of morphological changes.

The Morfac in Delft 3D accelerates morphodynamic updating (Lesser et al., 2004). This technique can significantly reduce real morphodynamic simulation time since morphodynamic change is much slower than the hydrodynamic changes (Roelvink and Walstra, 2004; Ranasinghe et al., 2011). This factor can be a constant or time-varying. It was decided to use a constant Morfac value in this study for simplicity. The selection of an appropriate Morfac value is essential for the accuracy of morphology simulations.

To explore the sensitivity of model simulations to the Morfac parameter, four test values were selected (Table 3). As annual historic estuary bathymetries are available, first a baseline one-year estuary morphology change simulation is carried out using the calibrated model with Morfac=1, taking 2002 bathymetry as the initial bathymetry. Then, the same simulations were repeated for Morfac values given in Table 3. Following that, the Brier Skill Score (BSS, eq.1) (Van Rijn et al., 2003; Sutherland et al., 2004) was used to compare those morphological change simulations with the baseline scenario in

order to select a suitable Morfac value for this application, without compromising the accuracy of the results.

$$BSS = 1 - \frac{\langle (Z_{MorfN} - Z_{Morf1})^2 \rangle}{\langle (Z_1 - Z_{Morf1})^2 \rangle} \quad (1)$$

Where Z_{morfN} =final bed level predicted by simulation with Morfac>1 (the tested values in Table 3); Z_{Morf1} =final bed level predicted by benchmark simulation (Morfac=1); and Z_1 =initial bed level.

Position of Table 1.

Position of Table 2.

Morphodynamic model validation

Before validation of the model against measured data, the important morphodynamic model parameters were calibrated.

The Deben Estuary consists of gavel-dominated mixed sand and gravel. Therefore, the bottom roughness should be should larger than that used for pure sand conditions. The validation process revealed that the Chèzy coefficient of $45\text{m}^{1/2}/\text{s}$ gives the best model performance. It was found that using the Chèzy coefficient does not influence the hydrodynamic model performance. We considered three sediment transport formulae available in Delft3D, which include both wave and current induced transport: Van Rijn (1993), Bijker (1971) and Soulsby (1997), in order to choose the best sediment transport formulae suitable for morphodynamic simulations in this study. However, it should be noted that the Van Rijn (1993) formula has not been validated for the coarse sediment present in the Deben Estuary ($d_{50} = 42.2\text{mm}$). A comparison between Van Rijn (1993) and Bijker (1971) formulae through a sensitivity analysis proved that the Bijker (1971) performs better in capturing morphodynamic change in the Deben Estuary. The sediment transport in the wave direction due to wave asymmetry is also included in Bijker (1971) formula through Bailard approach (Bailard, 1981). Based on the results of ten sensitivity tests, the Bijker (1971) formula provided the highest skill score, which was then used in all morphodynamic simulation here.

After selecting a suitable Morfac value, calibration parameters and the sediment transport formula, the model was then validated against its ability to reproduce morphodynamic change of the Deben inlet. The measured bathymetry from 2002 was used as the initial bathymetry of the model. The model was then used to simulate 2003 bathymetry, using measured wave and hydrodynamic boundary conditions during this period. The simulated final bathymetry was compared with the measured 2003 bathymetry, as shown in Fig. 10. The model correctly reproduced morphodynamic change of most areas of the inlet other than the down-drift areas of the ebb delta, which can be attributed to lack of sediment supply to the domain from updrift areas of the inlet. Discrepancies between modelled and measured morphodynamic change can also be attributed to (a) simplified sediment characteristics and distribution used in the model as a result of lack of sediment data; (b) model resolution; (c) complexity of the morphodynamic processes involved; and (c) inaccuracies of historic measurements (Burningham and French, 2006).

Position of Figure 10.

4. Morphodynamic response of Deben Estuary to future SLR

In order to consider the most likely future sea levels in the model domain by the end of the twenty first century, three SLR scenarios are considered: Low (LE), Medium (ME) and High (HE) green-house gas emission scenarios which will give the Mean Sea Level (MSL) rise around the Deben Estuary by 0.2m, 0.5m and 0.8m respectively by the end of this century.

In addition to SLR, the future wave climate conditions are also considered. The projection of future average incident wave conditions around Deben Estuary were taken from regionally downscaled wave data from the combined MRI-AGCM3.2H atmospheric global climate model and WAVEWATCH III wave model outputs (Mizuta et al., 2012; Shimura et al., 2015). Based on two time-slice experiments, 1979-2009 providing the present wave climate and 2075-2099 providing the future wave climate. It has been found that the average wave conditions around Suffolk area will not change significantly at the end of this century (Bennett et al., 2016; Yin, 2018) (Table 3). A comparison of current and future average wave conditions revealed that the average Hs decreased by 0.09% only in future while the peak wave period (Tp) decreased by 0.57%: both of which are insignificant. This means sea level change will be the governing parameter of morphodynamic change. Seasonal variation of wave climate was not considered so that annual

average wave climate conditions are used in model simulations. The freshwater discharge of River Deben is small compared to its tidal prism. Therefore, river flow is not considered in this study.

Position of Table 3.

By using the validated Deben Estuary model described in Section 3, numerical simulations of morphodynamic change of the Deben Estuary under three different future sea level scenarios were carried out. Historic and current morphodynamic change of Deben Estuary shows a cyclic behaviour where morphology of the outer estuary moves through three distinct states, described in Section 2.

Considering this, we will first investigate the impact of SLR on the ebb shoal when it is at its most unstable state (State C) by simulating one-year worth of morphodynamic change under three future sea level rise scenarios (Table 4). The 2002 bathymetry (Fig. 11) is used as the initial bathymetry for these simulations as it represents typical morphodynamic State C. Changes to hydrodynamic regime and morphodynamic response of the estuary to SLR will be discussed based on these results, as State C is the most unstable situation of the estuary.

We will then investigate the impact of SLR on during the full morphodynamic cycle of ebb delta by simulating morphology change of State A and B under HE sea level scenario. Morfac value of 12 was used for all simulations. The modelled scenarios are listed in Table 4.

Position of Table 4.

Position of Figure 11.

4.1. Hydrodynamic changes at State C due to SLR

Before investigating future morphodynamic change of State C due to SLR, hydrodynamic processes at the inlet under ‘present’ and ‘future’ sea level scenarios were investigated in detail, focusing on one spring tidal cycle. Instantaneous tidal current distributions at different stages of the highest spring tidal cycles is shown in the figures below.

Position of Figure 12.

Under the 'present' scenario, at the Slack spring tide Before Ebb (SBE, 09/09/2002 02:00AM), the tidal velocities are significantly low around the ebb delta (Fig. 12a). The average SBE seaward-directed current on the ebb delta (Fig. 16a) is around 0.2m/s but the current in the middle of the sand bar reaches 0.3m/s. A small anti-clockwise circulation can be seen on the north ebb shoal. On the downdrift shoal, a complex flow pattern occurs since the tidal current that propagates from southwest is divided into two directions when joining the slack current at ebb jet. A circular flow is also seen at the inner estuary where flood and ebb currents with similar magnitudes occurring at the flood (north of the flood delta) and ebb channels (south from the flood delta) respectively, as shown in Fig. 12a.

Under future sea level scenarios (Fig. 12b-d), the slack water current on the ebb shoal smooths towards the northeast. Similar process can be seen at the downdrift side of the ebb shoal, but the average flow velocity is higher compared to that under the present scenario. Flood currents in the main channel and throat have increased due to SLR and the flood current magnitudes in the inner estuary has almost doubled. This tidal current increases its magnitude as the SLR increases from LE to HE and reaches a maximum under the highest emission scenario

(TA_SC3C). The unbalanced flood and ebb tidal currents at the inner estuary shrink the circular current.

Four hours after SBE when the ebb tidal current has reached maximum during the spring ebb tidal phase (09/09/2002 06:00AM), the highest velocities occurred on the ebb shoal (Fig. 13). The largest flow velocity under the 'present' scenario (TA_SC0C) occurs at the middle of the main channel to ebb jet region, which is around 1.8m/s. Several small circular flow structures can be seen at the downdrift shoal. Under future sea level scenarios, the magnitude of the original ebb jet has slightly reduced, from 1.8m/s to around 1.3m/s under the HE scenario. The direction also switched from east south-east toward south (Fig. 13). Additionally, at the north side of the main tidal jet, a new ebb tidal jet current, whose offshore side contains much stronger currents than that at the onshore side, has formed. The magnitude of this current increases from LE to HE scenarios (Fig. 13b-d). Even though the primary ebb jet velocities under future scenarios are smaller than that under present scenario, the overall velocity magnitudes on the ebb shoal have increased as a result of SLR. The average velocity in the main channel has increased while the current at downdrift shoal is re-organized towards the south as a result of SLR.

Position of Figure 13.

At the Slack water time Before Flood tide (SBF, 09/09/2002 08:00AM) a weak ebb current flows along the main channel. With SLR, the velocity has been reduced while maintains a similar current pattern occurred under 'present' scenario (Fig. 14).

Position of Figure 14.

Under the 'present' scenario, the strongest currents during the SBF water time occur in the main channel as the geometry of the estuary converged the current to the main channel (Fig. 14a). However, after passing through the narrow channel the velocity veers at right angle towards offshore with a slight decrease in magnitude and then spread to the ebb jet region.

When sea level increases, most of the ebb delta is submerged even during low tide. Tidal currents in the main channel decreases as a result of the flow spreading over a wide area. Therefore, the SLR makes tidal currents gentle and wide-spread.

At the maximum flood phase (09/09/2002 12:00PM) flood currents in the throat area are stronger than that at the ebb shoal area. However, flow velocities reduce as sea level increases (Fig. 15). The distributions of velocities on the ebb shoal under the future sea level scenarios do not significantly differ from the 'present' scenario (TA_SC0C) whereas most differences occur at the inner estuary.

Position of Figure 15.

The tidally-induced residual currents (the average current over a tidal cycle) play a significant role on sediment transport, even though they may not always indicate net bedload transport (Bastos et al., 2003). Therefore, residual currents over a spring tidal cycle under 'present' and 'future' sea level scenarios were investigated in detail. The residual flows over a spring tidal cycle (09/09/2002 02:00AM to 12.00PM) under 'present' and 'future' scenarios are presented in Fig. 16.

Position of Figure 16.

Fig. 16 shows that the residual flows vary significantly under different SLR scenarios. Under the present scenario, the residual flow at the ebb jet region (offshore directed) is the most significant. However, shoreward-directed currents can be seen in the north tip of the ebb shoal (Fig. 16a). Additionally, a weaker seaward directed residual flow is seen on the north ebb shoal to form a new tidal ebb jet. These two opposing currents have created a small circular current in the area between the channel and the north ebb shoal.

This complex residual current distribution between the two main ebb jets on the ebb delta does not change significantly with SLR except for some small changes in current directions. The direction of the residual flow at the primary ebb jet has shifted from east south-east to south south-east as a result of SLR. The 'future' current magnitudes are lower than that under present scenario. The residual currents at a newly formed ebb jet has expanded and increased due to SLR (Fig. 15c-d). Also, the landward directed residual circle currents at north tip of ebb delta beside the throat have become more obvious (Fig. 16c-d).

At the downdrift side of the ebb delta, the residual currents become smaller and well-organised under future SLR scenarios.

Although there is a slight increase in seaward-directed current magnitude around the throat, the entire flow structure and magnitude at the inner estuary have not been significantly modified by the SLR. A similar observation can be seen around the throat of the inlet.

Hydrodynamic changes induced by SLR discussed above have shown that the Deben inlet will experience different hydrodynamic characteristics in future as a result of SLR. As the sea level rises, the entire outer estuary will potentially become more hydrodynamically active dynamic. The most notable difference is the formation of a new ebb jet and weakening of the main ebb current, which may have significant implications on future morphodynamic stability of the estuary, as will be investigated below.

4.2. Morphodynamic response of State C to SLR

Driven by the above hydrodynamic regimes, the morphodynamic changes to State C of the Deben inlet under difference scenarios based on the same initial bathymetry (Fig. 11) is investigated in detail. The final bathymetries under

‘present’ and ‘future’ SLR scenarios are shown in Fig. 17.

Under the present scenario (Fig. 17a), a breach (erosion) is developed at the middle of the north ebb shoal and the original ebb jet region experiences slight erosion.

Position of Figure 17.

With SLR, the ebb tidal delta becomes much more fragmented and the erosion is more obvious. The erosion at the north part of ebb shoal has developed under TA_SC1C scenario. Under both TA_SC2C and TA_SC3C scenarios where sea levels are higher, the breach is more pronounced and wider (Fig. 17b-d). The original ebb jet region seems to get much shallower as the sea level rises, particularly in the HE SLR scenario, there is a connection at this site between north ebb shoal and south ebb shoal. Due to the fragmented process of ebb shoal, the course of the main channel has been changed although the depth of main channel has not significantly changed. The original ebb jet region seems to begin to be infilled and the newly-formed ebb channel increased its depth. In terms of inner estuary, there is no significant change either in the tidal channel or on the flood tidal delta, which seems to maintain relatively stable regardless of SLR.

In order to investigate morphodynamic changes under different SLR scenarios in detail, cumulative erosion/accretion of the inlet was investigated further. The resultant cumulative erosion/accretion patterns in the estuary for all current and future sea level scenarios are shown in Fig. 18. It is seen that the bed level changes under different SLR scenarios are different and the most significant differences occurred at the ebb tidal delta and the main channel.

Under the TA_SC0C scenario, most erosion occurred at the middle section of the ebb shoal while sediment is transported and deposited at the seaward side of the ebb jet region resulting in accretion outside the delta (Fig. 18a). The erosion/accretion at this primary ebb jet position indicates that the net offshore sediment transport occurs along the primary ebb jet occupying the majority morphological changes on the ebb shoal. The most significant accretion occurred approximately at 600m offshore of the coastline probably due to reduced ebb velocity resulted from expansion of flow field at the end of ebb jet region (Fig. 12). Although a slight erosion can be seen at the north ebb shoal, it is not significant enough to form a new channel. No obvious erosion/accretion pattern can be observed in the downdrift or throat areas.

Morphodynamic changes observed in the ebb jet area under TA_SC1C scenario is not significantly different to that under the TA_SC0C scenario (Fig. 18b). The primary ebb jet region has experienced slight morphodynamic changes compared to TA_SC0C although the most significant erosion position has not changed. The dynamic area at ebb jet region in this scenario has been slightly expanded compared to that in TA_SC0C scenario. A new eroded and accreted area at the north ebb shoal appears in this scenario although those changes are not very significant (Fig. 18b).

Fig. 18c shows that under TA_SC2C scenario, the overall areas of accretion/erosion are much wide-spread than that under the previous scenarios. The primary ebb channel will experience less erosion while the new erosion/accretion pattern at the north ebb shoal created a secondary channel. The erosion/accretion pattern at the original ebb jet region has moved to the south. Meanwhile, the newly-formed channel at the northern part of ebb shoal, whose seaward side accumulates more sediment due to the SLR, has attracted a comparable erosion/accretion amount compared to that in the primary ebb jet region (Fig. 18c). The deposition of sediment offshore of the new channel has increased significantly: in some areas, accretion as large as 3m can be seen. Morphological changes at the new channel

may have been initiated by the sediment starving of the offshore side. This can be explained by the distributions of ebb tidal current in the new channel area where velocity magnitudes at the offshore side are much larger than the estuary side (Fig. 13).

The landward sediment transport at the north tip of ebb delta under this scenario (erosion offshore and deposition onshore shown in Fig. 18c) may be partially due to the increase of residual tidal flow (Fig. 16c). However, since the residual tidal flow does not change significantly as a result of sea level rise, the most notable contribution may be the reduction of slack water velocity before spring ebb tide (SBE) (Fig. 12). The low tidal currents may have provided sufficient time for the fine sediment to deposit further onshore.

Under the High Emission (HE) scenario TA_SC3C, the entire ebb delta has experienced significant erosion and a new channel has been formed at the north ebb shoal (Fig. 18d). Although the bed changes of the original ebb jet region are minimal in this scenario, the most notable observation is the increased erosion of the new channel which has cut across the ebb tidal delta (Fig. 18d).

In the original ebb jet region, both the extent and intensity of morphological change has reduced, which indicates transport of sediment further downstream to the south, leading to a smaller deposition area at the tip of the ebb shoal. Meanwhile, the newly-formed channel at the north side of ebb shoal has eventually replaced the original ebb channel. The strengthening of the landward residual current at the north tip of the ebb shoal with the increase of SLR (Fig. 16d) may have brought more sediment to the main channel, thus infilling the channel and eroding the northern part of the ebb shoal.

The acceleration of sediment starving of the ebb delta due to SLR may result in some changes to the longshore sediment transport regime along the mouth of the inlet thus resulting changes to the current cyclic morphodynamic behaviour of the inlet. If the north ebb shoal is not supplied with adequate amount of sediment from the updrift coastline, it is possible that the ebb shoal will be further eroded. Although, it has been reported that the delta is supplied sediment from Orford Ness, a large sediment feature located to the north of the estuary (HR Wallingford, 2002), accelerated sediment loss may not allow the ebb shoal and the delta to recover.

Position of Figure 18.

Position of Figure 19.

To investigate the spatial variation of morphological change in State C in detail several cross sections at the inlet are selected (red lines in Fig. 19). The cross section 'BR1' is at the primary ebb jet and cross section 'BR2' is located the secondary breach position. Section 'DD' is located at the downdrift beach and the throat cross section is 'TR'. All selected cross-sections extend no more than 700m offshore from the coastline as the bed level changes in the deeper areas are insignificant.

The bed level changes of these four cross sections under current and future sea level scenarios are shown in Fig. 20. At the throat (TR) cross section (Fig. 20a), the offshore directed sediment transport increased as the sea level increases from LE to HE scenario thus widening and flattening the throat.

At the secondary breach section (BR2), shoal erosion increases as the sea level increases from LE to HE scenario (Fig. 20b)

which results in reducing the crest of the shoal, which led to the breach. The opposite is seen at BR1 where lowest emission scenario sea level has caused the least erosion (Fig. 20c). However, although accumulation is slightly higher at DD under HE, the differences under different SLR scenarios are not significant (Fig. 20d).

Position of Figure 20.

To explore changes to wave propagation (Fig. 21) as a result of higher sea levels and their contribution the inlet morphodynamics, we investigated H_s at the ebb delta position (red dot EW in Fig. 19). The nearshore H_s increases with increase in sea level. The mean H_s value has increased by 13% from the present scenario TA_SC0C to HE future scenario TA_SC3C. It will be correct to assume that the rise in H_s may contribute to morphodynamic changes primarily induced by increased sea levels in future.

Position of Figure 21.

In summary, State C of the Deben estuary inlet will have significant consequences as a result of SLR. Under both ME and HE SLR scenarios, a secondary channel will form as a result of a breach of the ebb shoal, further weakening the shoal. This may prevent the inlet from evolving into the next phase of its morphodynamic cycle, unless sediment supply from the updrift beach is significantly increased in future.

To gain insights into the future of the full cycle of current morphodynamic evolution of the inlet, the following section investigates the response of the other two morphodynamic states of the inlet.

4.3. Morphodynamic response of the State A of the inlet to SLR

The Deben model was used to investigate the morphodynamic response of the inlet to SLR when it is in State A, the most stable state of the inlet. A similar modelling approach where 1-year simulation is carried out, taking initial bathymetry as the 1998 measured bathymetry which represents State A and same sea level, wave and tidal conditions used when modelling State

C above. Fig. 22 shows cumulative bed change over 1 year. In this case, simulations were done only for HE SLR scenario.

Position of Figure 22.

The results reveal that SLR certainly increases morphodynamic activity of the inlet compared to current situation however, the changes are less intense than that for State C (Fig. 18d). Under HE SLR scenario, morphodynamic activities are concentrated towards the north of the inlet as opposed to the current situation where the southern part of the shoal is more active. Two narrow erosion areas can be seen in the northern side of the shoal, which may have the potential to destabilise the shoal.

4.4. Morphodynamic response of the State B of the inlet to SLR

State B is the transient morphodynamic state of the Deben inlet where the inlet evolves from the most stable State A to the unstable State C. Currently at this stage, the ebb shoal show signs of erosion at several places, finally breaching and

shortening when reaches State C. The morphodynamic change after 1-year simulation starting from State B initial bathymetry (year 2000 measured bathymetry) and HE SLR scenario is shown in Fig. 23.

Position of Figure 23.

Compared to other two morphodynamic states of the inlet State B shows the least amount of change as a result of SLR.

Although erosion all along the shoal will increase compared to the current state, the lowering of shoal is small, other than at the northern most point of the shoal where it connects with updrift shoreline. The eroded material has deposited just offshore of the shoal area.

Although future climate change negatively impacts all three morphodynamic states of the estuary, State C is proved to be the most affected by SLR. Further fragmentation and drowning of the delta may not allow it to evolve into a dynamically stable morphodynamic state (as in State A in current situation) thus breaking the cyclic morphodynamic behaviour in future unless sediment influx from updrift coast is significantly increased.

In all three morphodynamic states under SLR, the ebb shoal was found the most vulnerable feature of the Deben Estuary. Although morphodynamic change of wave-dominated estuarine spits and shoals take place as a result of erosion of the seaward side, the Deben Estuary ebb shoal predominantly erodes from the estuary side (Figs. 20b &c). This could be explained by the meso-tidal regime of the estuary where ebb tidal currents as strong as 2.0m/s are generated at spring tide while wave forcing is weak. Although ebb tidal velocities in the channel are equally strong, it can be seen that the tidal channel largely remains unchanged due to SLR, which may be due to the fact that the channel consists of significantly coarser sediment than the rest of the estuary.

5. Conclusions

The morphodynamic response of a meso-tidal, gravel dominated Deben estuary inlet to SLR is investigated using the state-of-the-art process-based Delft 3D numerical model. The model, carefully validated against measured historic wave, hydrodynamic and morphodynamic data shows that it can satisfactorily reproduce future morphodynamic variability of the Deben estuary inlet. We followed the ‘snapshot’ approach

used by Duong et al. (2017) where a future time window of one year at the end of this century is modelled for our investigation, using projected future sea levels for the UK from UKCP09 and wave conditions from a global wave model.

Investigation of the inlet hydrodynamic regime under future sea level scenarios has shown that the ebb tidal currents around the ebb shoal will be larger in future. Also, a new ebb jet is formed at the northern part of the shoal while the velocities in the existing ebb jet will become smaller.

Investigation of morphodynamic response of the Deben Estuary to the impacts of climate change shows that there will be significant changes to the future morphodynamic behaviour of the estuary inlet as a result of global climate variabilities. The ebb shoal of the estuary will become more dynamic and unstable in future. Since changes to future wave conditions as a result of climate change is insignificant around the study site, the primary cause for morphodynamic change is found to be to the SLR. Model results reveal that there will be a new secondary channel formed at the north ebb shoal while the erosion at the original ebb jet region will be reduced with the increase rate of SLR. In the high emission SLR scenario, the

ebb tidal delta is fragmented mainly as a result of the newly formed small channel, forcing it into a more fragmentation and instability.

In the inner estuary, neither hydrodynamics nor morphodynamics experience significant changes as a result of future SLR when compared to the changes observed at the inlet. The observed changes can be attributed to the changes occurred to the hydrodynamic regime as a result of the fragmented ebb shoal. It was also found that the changes to residual tidal currents in the inner estuary and to the tidal prism as a result of SLR are not large thus minimising SLR impacts on the inner estuary. The impacts of waves on the inner estuary are not significant. This can be explained by the restricted wave entrance to the inner estuary from the narrow throat.

In its current form, the estuary revolves around three distinct morphodynamic states where the ebb shoal cycles between ‘fully formed’, ‘transient’ and ‘fragmented’ states (Burningham and French, 2006). Our modelling suggests that one consequence of SLR will be to increase the extent of fragmentation and partial drowning of the ebb shoal when it is at the most unstable ‘fragmented (State C) state. A natural

consequence of this is likely to be moving the inlet away from its current quasi-stable cyclic behaviour altogether, unless sediment supply from the updrift coast significantly increase in future, which is an unlikely scenario. Furthermore, the unique spatial sediment distribution and meso-tidal regime force the weakened shoal to move offshore. It should be noted that the simplified modelling approach used in this study did not consider any potential changes to the sediment supply and lateral transport regime as a result of SLR, which may have some implications on future morphodynamics of the estuary. Also, the ‘snapshot’ approach used here does not allow for a full investigation of gradual adaptation of the estuary to climate change under an abundant sediment influx scenario.

Although the present study is focused on the Deben Estuary inlet, the results may be of value to other estuaries with similar hydrodynamic and morphodynamic characteristics. Also, the modelling approach developed in this study are easily transferable to any other site, once site specific bathymetries and boundary conditions for numerical simulations are established. However, as a result of complex, localised nature of hydrodynamics and morphodynamics of estuary systems, site-specific studies are needed to investigate future morphodynamic behaviour of a specific estuary.

Our findings agree with the findings of Van Goor et al. (2003) and Dissanayake et al. (2009) where they observed inlets, in the event of SLR, will drown or degenerate if they have sediment. However, it should be noted that the unique gravel dominated mesotidal regime and the complex cyclic morphodynamic variability of the inlet does not allow direct comparison of our results with inlet stability models reported in literature (e.g. Bruun, 1978; Duong et al., 2017).

Acknowledgment

The authors thank the UK Natural Environment Research Council (NERC) funded iCOASST (NE/J005606/1) project for providing the bathymetry data, British Oceanography Data Centre (BODC) and CEFAS for providing tide and wave data respectively. We also acknowledge Dr. Nobuhito Mori at Disaster Prevention Research Institute of Kyoto University for providing projected global wave data from Japanese Meteorological Research Institute and the Japan Meteorological Agency (MRI-JMA). The first author acknowledges the China Scholarship Council (CSC) and the College of Engineering of Swansea University for jointly funding his PhD study at Swansea University.

References

- Anthony, E.J., Levoy, F., Monfort, O., 2004. Morphodynamics of intertidal bars on a megatidal beach, Merlimont, Northern France. *Marine Geology*, 208: 73-100.
- Bailard, J.A., 1981. An energetics total sediment transport model for plane sloping beaches. *Journal of geophysical research* 86 (C11): 10938-10954.
- Bastos, A., Collins, M., Kenyon, N., 2003. Water and sediment movement around a coastal headland: Portland Bill, southern UK. *Ocean Dynamics*, 53, 309-321.
- Bennett, W.G., Karunarathna, H., Mori, N., Reeve, D.E., 2016. Climate change impacts on future wave climate around the UK. *Journal of Marine Science and Engineering*, 4, 78.
- Bijker, E., 1971. Longshore transport computation. *ASCE Journal of Waterway, Port, Coastal and Ocean Engineering*, 97, pp. 687-701.
- Booij, N., Ris, R.C. and Holthuijsen, L.H., 1999. A third-generation wave model for coastal regions, Part I, Model description and validation. *Journal of Geophysical Research* 104 (C4): 7649–7666.
- Boothroyd, J.C., 1985. Tidal inlets and tidal deltas, in: Davis Jr., R.A. (Ed.), *Coastal Sedimentary Environments*. Springer-Verlag, New York, pp. 445-532.

- Bruun, P., 1978. Stability of tidal inlets – Theory and engineering. Developments in Geotechnical Engineering, Elsevier Scientific, Amsterdam, 510p.
- Burningham, H. and French, J., 2006. Morphodynamic behaviour of a mixed sand–gravel ebb-tidal delta: Deben estuary, Suffolk, UK. Marine Geology, 225(1-4): 23-44.
- Collins, J., 1972. Prediction of shallow water spectra. Journal of Geophysical Research, 77(15): 2693-2707.
- DEFRA, 2008. Development and Demonstration of Systems-Based Estuary Simulators. R&D Technical Report FD2117/TR. London: DEFRA.
- Dickson, M., Walkden, M., Hall, J.W., 2007. Systematic impacts of climate change on an eroding coastal region over the twenty-first century. Climatic Change 84(2):141–166.
- Dissanayake, D.M.P.K., Ranasinghe, R. and Roelvink, J.A. 2009. Effects of sea level rise in tidal inlet evolution, Journal of Coastal Research, SI56, 942-946.
- Dissanayake, P. K. 2011. Modelling morphological response of large tidal inlet systems to sea level rise. Ph.D. thesis. Delft University of Technology.
- Dissanayake, P., Brown, J. M., Karunarathna, H., 2014. Modelling storm-induced beach/dune evolution: Sefton

coast, Liverpool Bay, UK. *Marine Geology*, 357, 225-242.

Douglas, B.C., Kearney, M.S., Leatherman, S.P., 2001. Sea level rise: history and consequences. Academic Press, San Diego, US, pp. 232.

Duong T.M., Ranasinghe, R., Luijendijk, A. and Walstra, D. 2017. Assessing climate change impacts on the stability of small tidal inlets: Part 1 - Data poor environments, *Marine Geology*, 390, 331-346.

Duong, T.M. et al. 2018. Assessing climate change impacts on the stability of small tidal inlets: Part 2 - Data rich environments, *Marine Geology*, 395, 65-81.

Finley, R. J. 1978. Ebb-tidal delta morphology and sediment supply in relation to seasonal wave energy flux, North Inlet, South Carolina. *Journal of Sedimentary Petrology*, 48, 227-238.

Hasselmann, K., Barnett, T.P., et al., 1973. Measurements of wind-wave growth and swell decay during the Joint North Sea Wave Project (JONSWAP). Hamburg.

Houghton, G.T., Ding, Y., Griggs, D.J., Noguer, M., Van der Linden, P.J., Dai, X., Maskell, K., Johnson, C.A., 2001. *Climate Change Scientific Basis, Contribution of Working Group 1 to the third Assessment report of the*

Intergovernmental Panel of Climate Change (IPCC),
Cambridge University Press, UK, pp.74-77.

HR Wallingford, 2002. Southern North Sea Sediment Transport
Study (phase 2). HR Wallingford Report EX, pp.4526.

Hulme, M., Jenkins, G.J., Lu, X., Turnpenny, J.R., Mitchell, T.D.,
Jones, R.G., Lowe, J., Murphy, J.M., Hassell, D.,
Boorman, P., McDonald, R. and Hill, S., 2002. Climate
Change Scenarios for the United Kingdom: The
UKCIP02 Scientific Report, Tyndall Centre for Climate
Change Research, School of Environmental Sciences,
University of East Anglia, Norwich, UK. 120pp.

Hydrographic Office, 2000. Admiralty tide tables: United
Kingdom and Ireland (including European channel
ports). Hydrographer of the Navy, pp.440.

Karunarathna, H. and Reeve, D.E., 2008. A Boolean approach
to prediction of long-term evolution of estuary
morphology. *Journal of Coastal Research*, 24(2B), 51-
61.

Karunarathna, H. Reeve D.E. and Spivack, M. 2008. Long-term
morphodynamic evolution of estuaries: An inverse
problem, *Estuarine Coastal and Shelf Science*, 77, 385-
395.

Lesser, G., Roelvink, J., van Kester, J. and Stelling, G., 2004.
Development and validation of a three-dimensional

morphological model. *Coastal Engineering*, 51(8-9):
883-915.

Lowe, J. A., Howard, T. P., Pardaens, A., Tinker, J., Holt, J.,
Wakelin, S., Milne, G., Leake J., Wolf, J., Horsburgh,
K., Reeder, T., Jenkins, G., Ridley, J., Dye, S., Bradley,
S., 2009. UK Climate Projections science report:
Marine and coastal projections. Met Office Hadley
Centre, Exeter, UK.

Madsen, O., Poon, Y.K., Graber, H.C., 1988. Spectral wave
attenuation by bottom friction: Theory. In *Proceedings
21th international Conference Coastal Engineering*.
ASCE, pp: 492-504.

Mizuta, R., Yoshimura, H., Endo, H., Ose, T., Kamiguchi, K.,
Hosaka, M., and et al., 2012. Climate Simulations
Using MRI-AGCM3.2 with 20-km Grid. *Journal of the
Meteorological Society of Japan*, 90, 233–258.

Murphy, A.H., Epstein, E.S., 1989. Skill scores and correlation
coefficients in model verification. *Monthly Weather
Review*, 117, 572–581.

Posford Duvivier, 1999. *Suffolk Estuarine Strategies: Deben
Estuary. Strategy Report: Phase 2 volume 1 Main
Report*. Peterborough: Environment Agency: Anglian
Region, pp. 5-20.

- Ranasinghe, R., McLoughlin, R., Short, A. and Symonds, G.,
2004. The Southern Oscillation Index, wave climate,
and beach rotation. *Marine Geology*, 204(3-4): 273-287.
- Ranasinghe, R., Swinkels, C, Luijendijk, A., Roelvink, D.,
Boshoom, J., Stive, M., Walstra, D.J., 2011.
Morphodynamic upscaling with the MORFAC
approach: Dependencies and sensitivities. *Coastal
Engineering*. 58. 806-811.
- Ranasinghe, R. 2016. Assessing climate change impacts on
open sandy coasts: A review, *Earth Science Reviews*,
160, 320-332.
- Reeve, D. E. and Karunaratna, H., 2009. On the prediction of
long-term morphodynamic response of estuarine
systems to sea level rise and human interference.
Continental Shelf Research, 29 (7), 938-950.
- Roelvink, J. A. and D. J. R. Walstra, 2004. Keeping it simple
by using complex models. In *Proceeding of the 6th
International Conference on Hydro-Science and
Engineering. Advance in Hydro-Science and
Engineering*, vol. page p. 12. Brisbane, Australia.
- Roelvink, J. A., 2006. Coastal morphodynamic evolution
techniques. *Coastal Engineering*, 53(2-3), 277-287.
- Shimura, T., Mori, N., Mase, H., 2015. Future projection of
ocean wave climate: analysis of SST impacts on wave

climate changes in the Western North Pacific. *Journal of Climate*, 18: 3171-3190.

Sutherland, J., Peet, A.H., and Soulsby, R.L., 2004. Evaluating the performance of morphological models, *Coastal Engineering* 51, 917-939.

van der Wegen, M., and Roelvink, J. A., 2012. Reproduction of estuarine bathymetry by means of a process-based model: Western Scheldt case study, the Netherlands. *Geomorphology*, 179, 152–167.

Van Goor, M.A., Zitman, J.T., Wang, Z.B. and Stive, M.J.F. 2003. Impacts of sea level rise on the morphological equilibrium state of tidal inlets, *Marine Geology*, 202, 211-227.

Van Rijn, L.C., Walstra, D. J. R., Grasmeyer, B., Sutherland, J., Pan, S., Sierra, J.P., 2003. The predictability of cross-shore bed evolution of sandy beaches at the time scale of storms and seasons using process-based profile models. *Coastal engineering*, 47, 295-327.

Yin, Y., 2018. Morphodynamic response of estuaries to climate change. Ph.D thesis. Swansea University, Swansea, UK.

Zacharioudaki, A., Reeve, D.E., 2011. Shoreline evolution under climate change wave scenarios. *Climate change*, 108, 72-105.

Table 1 – The skill performances in different Morfac values used in the sensitivity analysis

| | Morfac=10 | Morfac=12 | Morfac=20 | Morfac=24 |
|-----|-----------|-----------|-----------|-----------|
| BSS | 0.75 | 0.72 | 0.55 | 0.46 |

ACCEPTED MANUSCRIPT

Table 2 – BSS classification (van Rijn, 2003)

| Qualification | Morphology BSS |
|-----------------|----------------|
| Excellent | 1.0-0.8 |
| Good | 0.8-0.6 |
| Reasonable/fair | 0.6-0.3 |
| Poor | 0.3-0 |
| Bad | <0 |

ACCEPTED MANUSCRIPT

Table 3. The present and future average wave conditions in the Deben Estuary based on the global wave model projection. (H_s stands for the significant wave height; T_p is the peak wave period; Dir is the wave propagation direction).

| | | Present/Future | | |
|---------------------|--------|----------------|-----------|-------------|
| | | Hs(m) | T_p (s) | Dir(Degree) |
| Total averaged | | 1.1/1.1 | 5.27/5.24 | 50/50 |
| Seasonally averaged | Spring | 1.1/1.1 | 5.3/5.4 | 45/45 |
| | Summer | 0.8/0.8 | 5.2/5.0 | 270/270 |
| | Autumn | 1.1/1.1 | 5.2/5.2 | 270/270 |
| | Winter | 1.4/1.4 | 5.4/5.4 | 45/45 |
| Monthly averaged | Jan | 1.39/1.45 | 5.28/5.50 | 45/45 |
| | Feb | 1.30/1.36 | 5.38/5.34 | 45/45 |
| | Mar | 1.25/1.29 | 5.38/5.41 | 45/45 |
| | Apr | 1.11/1.14 | 5.26/5.41 | 45/45 |
| | May | 0.99/1.00 | 5.28/5.29 | 270/270 |
| | Jun | 0.93/0.87 | 5.28/5.11 | 270/270 |
| | Jul | 0.80/0.75 | 5.16/5.04 | 270/270 |
| | Aug | 0.79/0.74 | 5.05/4.98 | 270/270 |
| | Sep | 0.99/0.88 | 5.19/5.06 | 270/270 |
| | Oct | 1.06/1.11 | 5.22/5.19 | 270/270 |
| | Nov | 1.20/1.25 | 5.25/5.28 | 45/45 |
| | Dec | 1.49/1.42 | 5.51/5.31 | 45/45 |

Table 4 – All simulation scenarios based on SLR and the wave boundary conditions used in this study

| Wave condition | Sea level | Inlet State | Simulation Scenario |
|----------------|---------------------|-------------|---------------------|
| TA | BA (= 0) | C | TA_SC0C |
| TA | LE SLR (0.2m) (= 1) | C | TA_SC1C |
| TA | ME SLR (0.5m) (= 2) | C | TA_SC2C |
| TA | HE SLR (0.8m) (= 3) | C | TA_SC3C |
| TA | BA (= 0) | A | TA_SC0A |
| TA | HE SLR (0.8m) (= 3) | A | TA_SC3A |
| TA | BA (= 0) | B | TA_SC0B |
| TA | HE SLR (0.8m) (= 3) | B | TA_SC3B |

[TA= Average Wave Condition; BA=Baseline model with Current Sea Level; LE= Low Emission scenario SLR; ME = Medium Emission scenario SLR; HE = High Emission scenario SLR; SC=Scenario].

Research Highlights

1. Climate change impacts on a meso-tidal, gravel dominated Deben estuary inlet is studied.
2. The inlet morphodynamics is sensitive to sea level rise scenario and littoral transport regime.
3. The ebb delta of the estuary will be unstable and may drown as a result of sea level rise thus deviating from its present cyclic evolution
4. The methods and model used here can be easily transferable to other inlets

ACCEPTED MANUSCRIPT

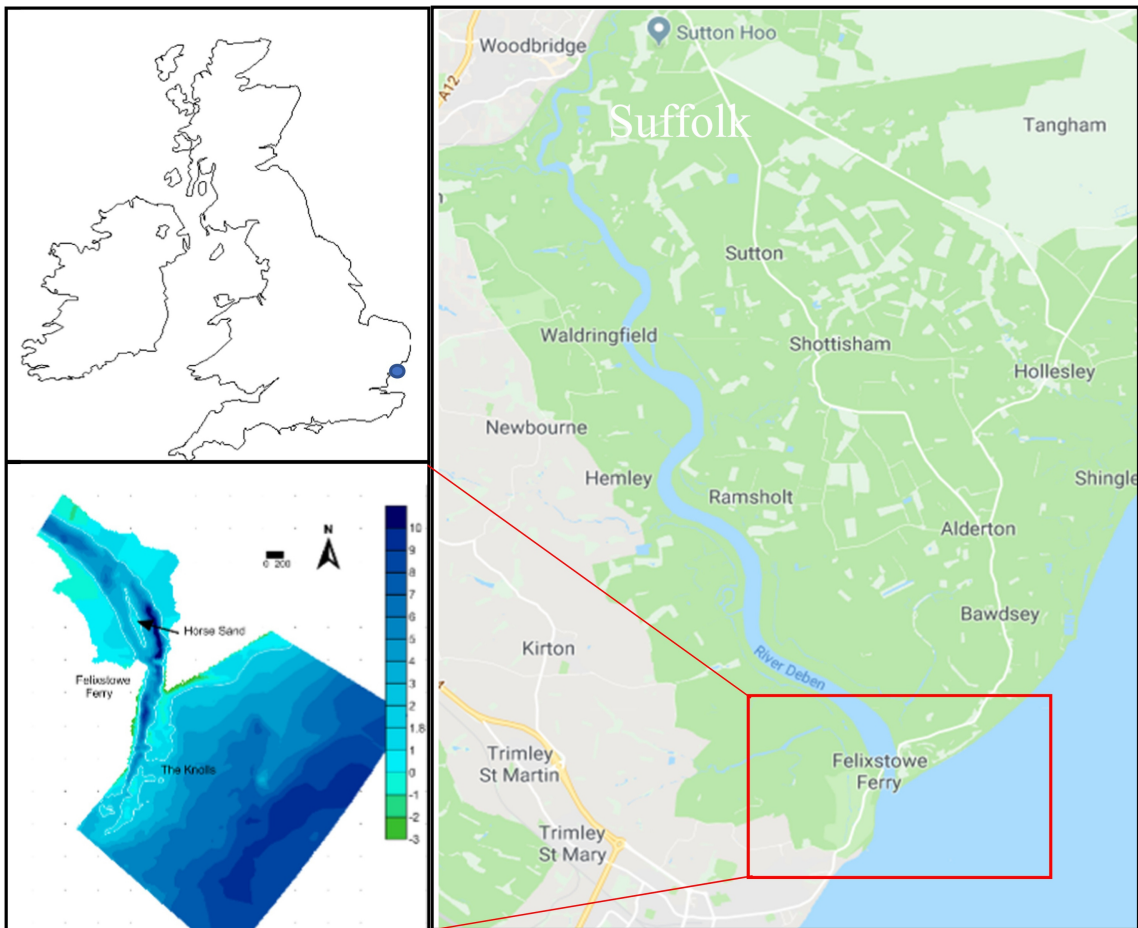


Figure 1

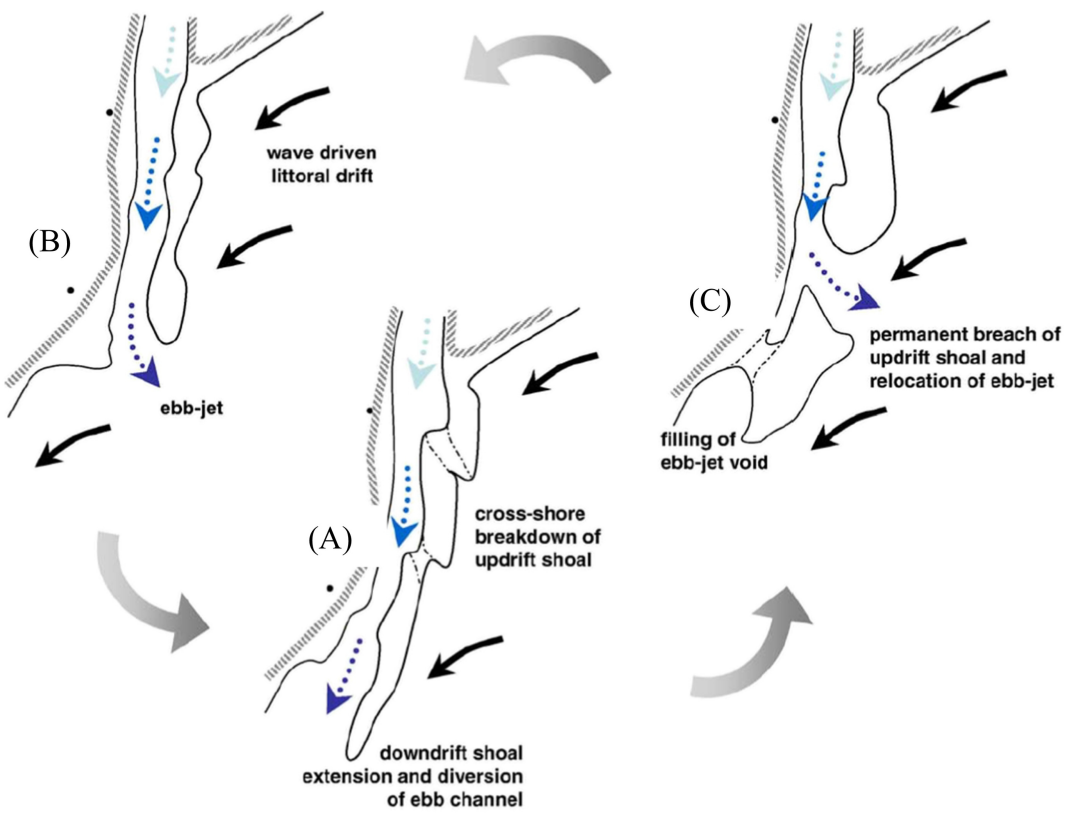


Figure 2

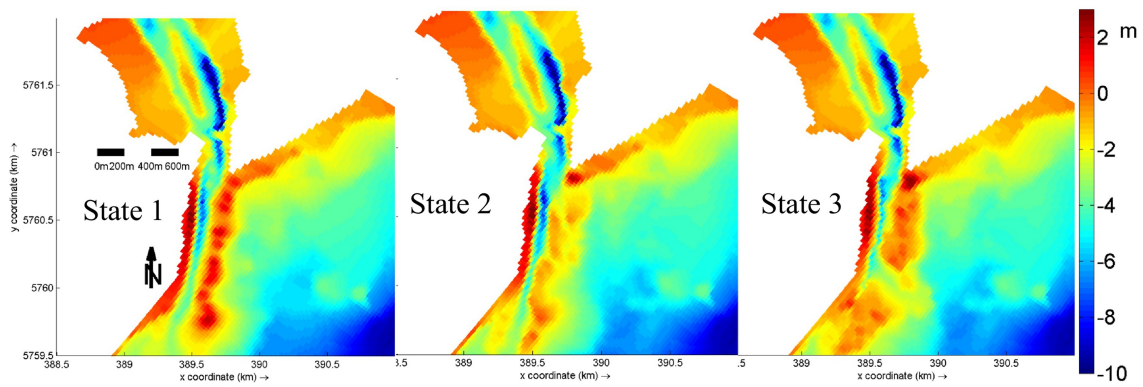


Figure 3

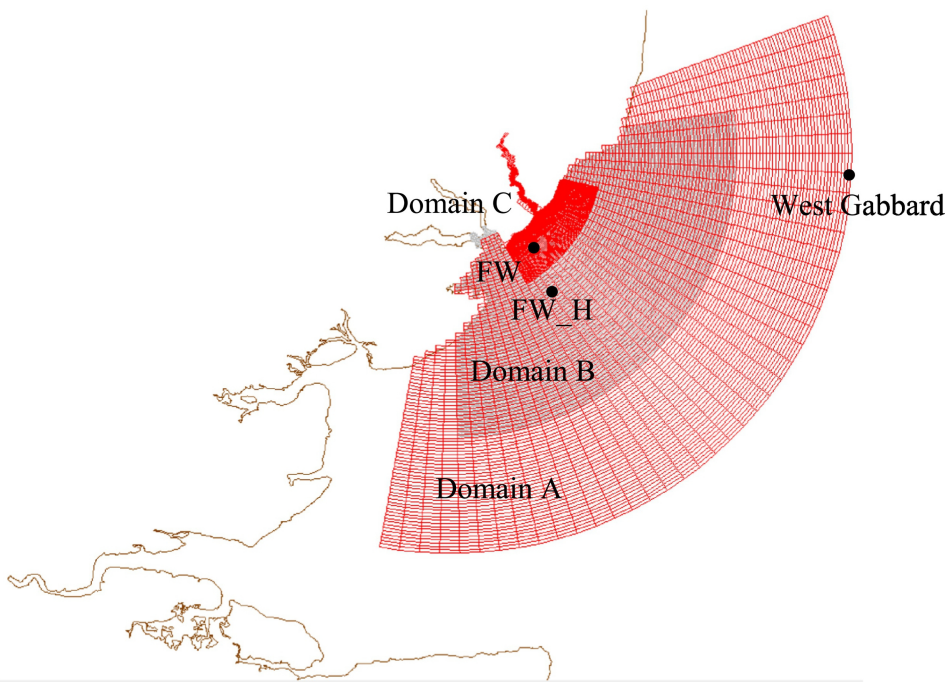


Figure 4

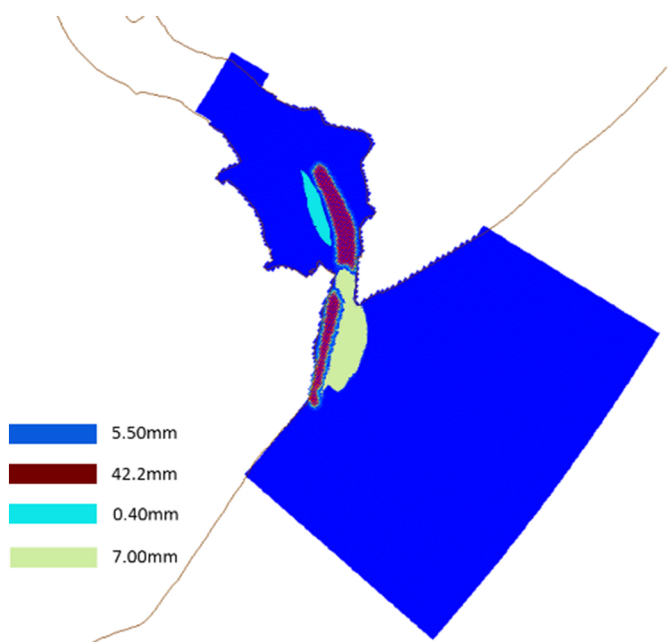


Figure 5

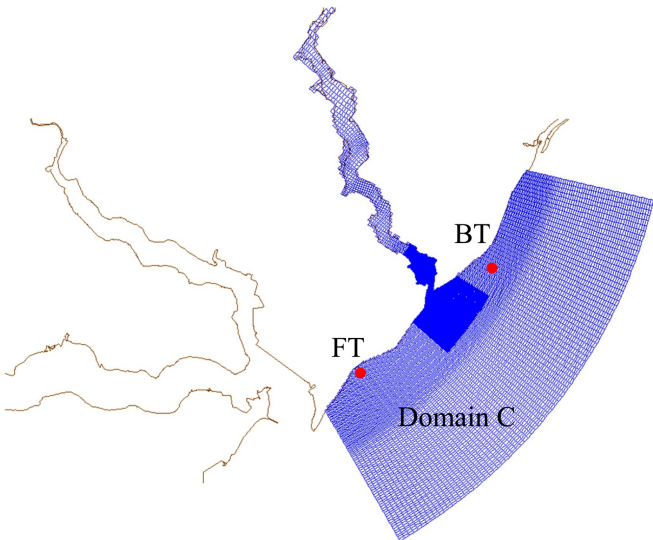


Figure 6

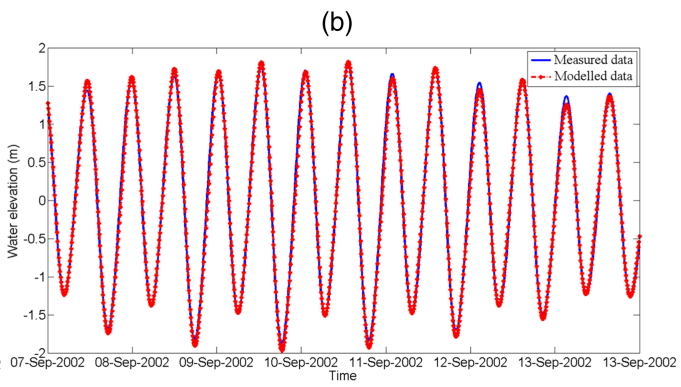
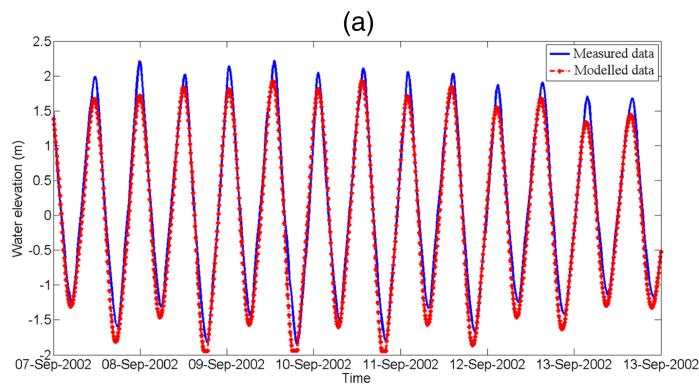


Figure 7

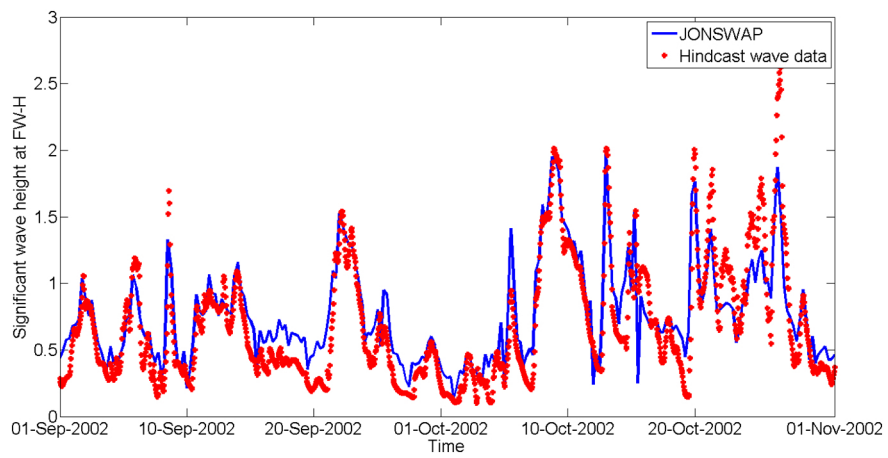


Figure 8

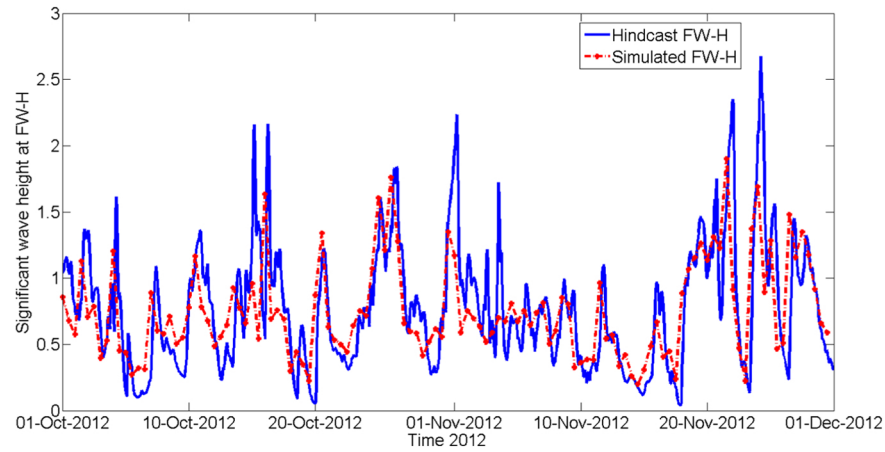
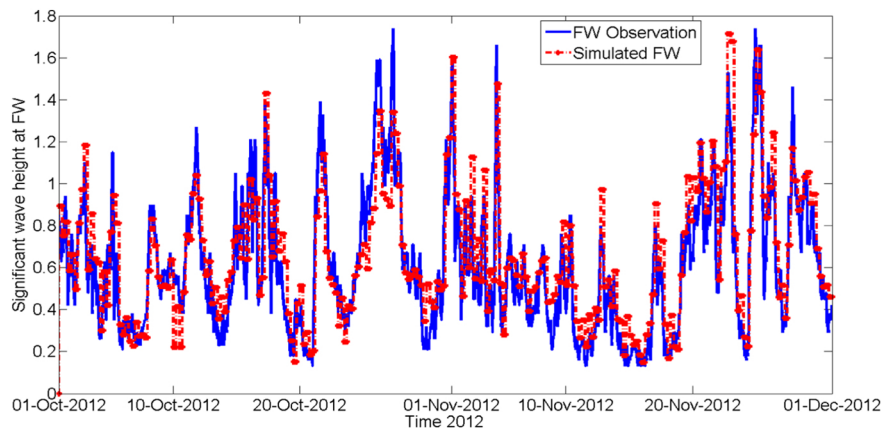


Figure 9

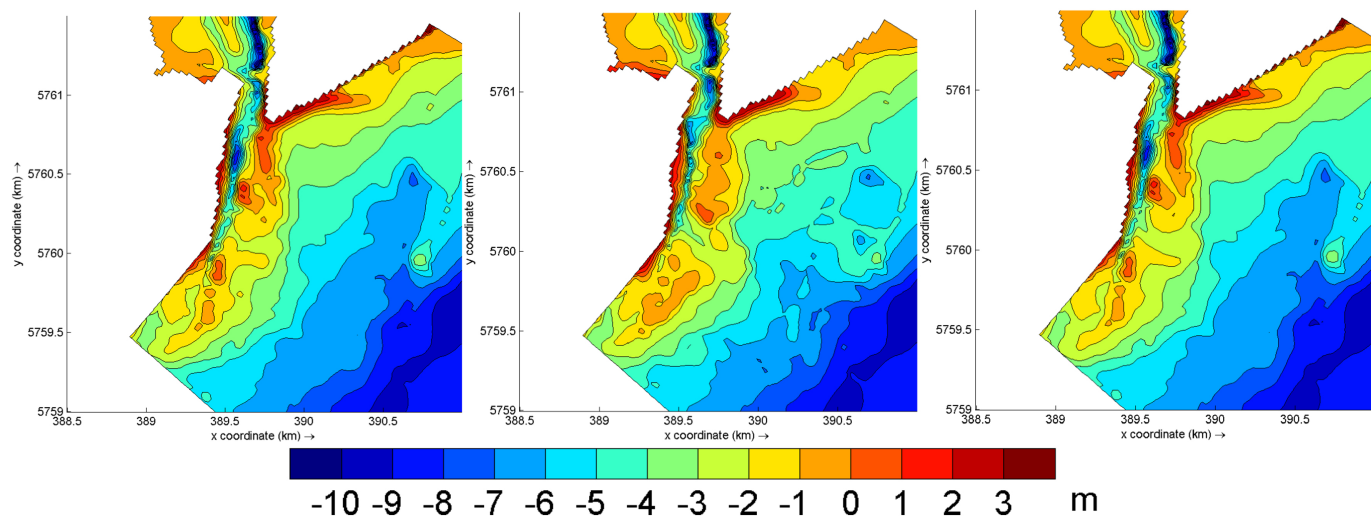


Figure 10

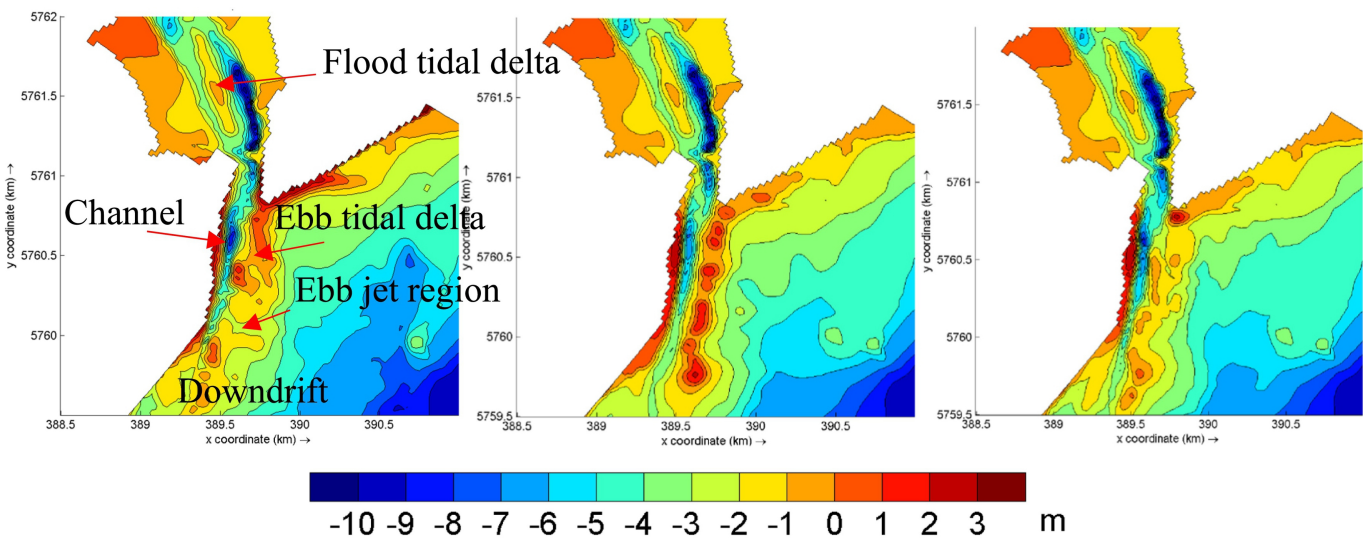


Figure 11

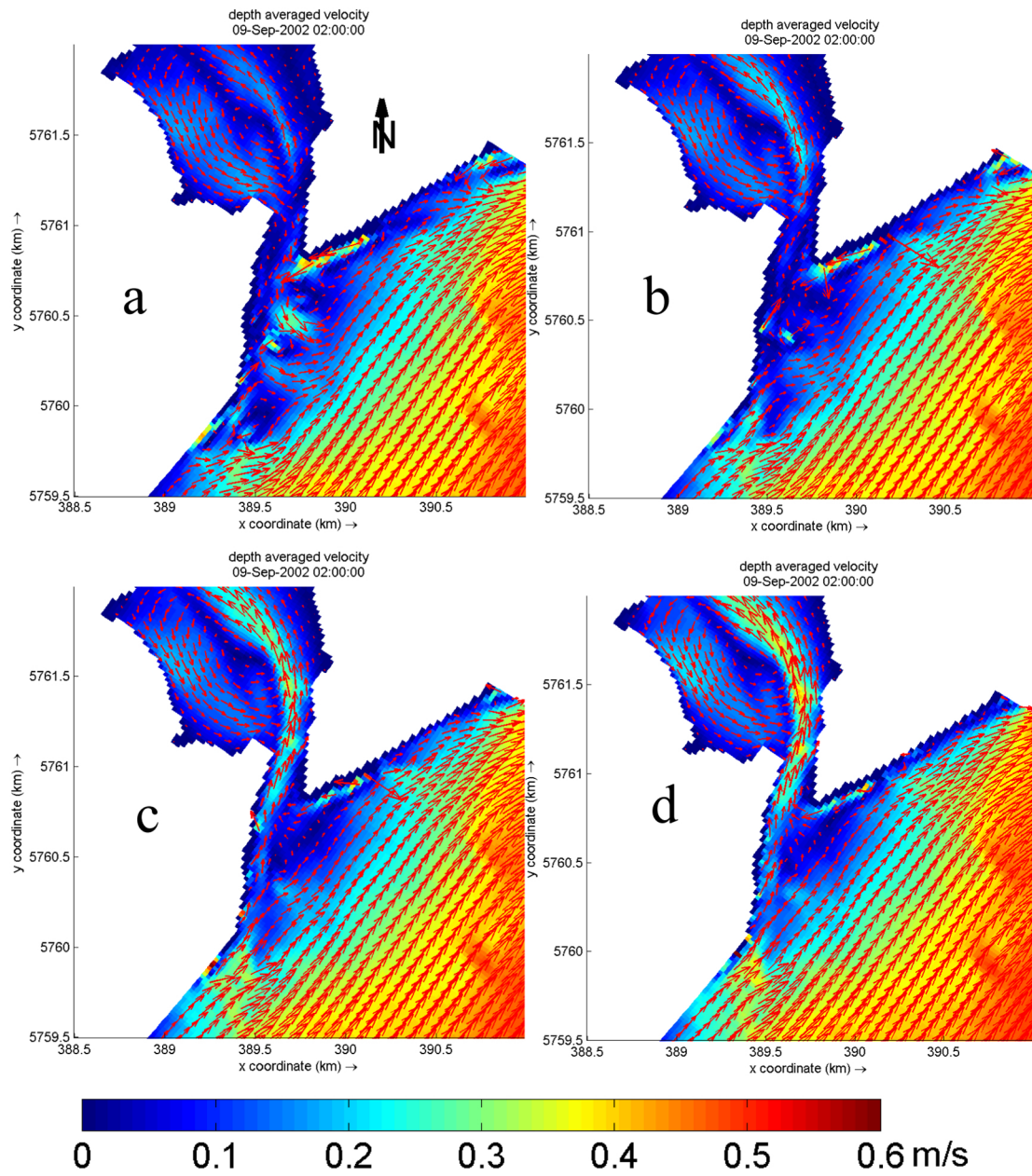


Figure 12

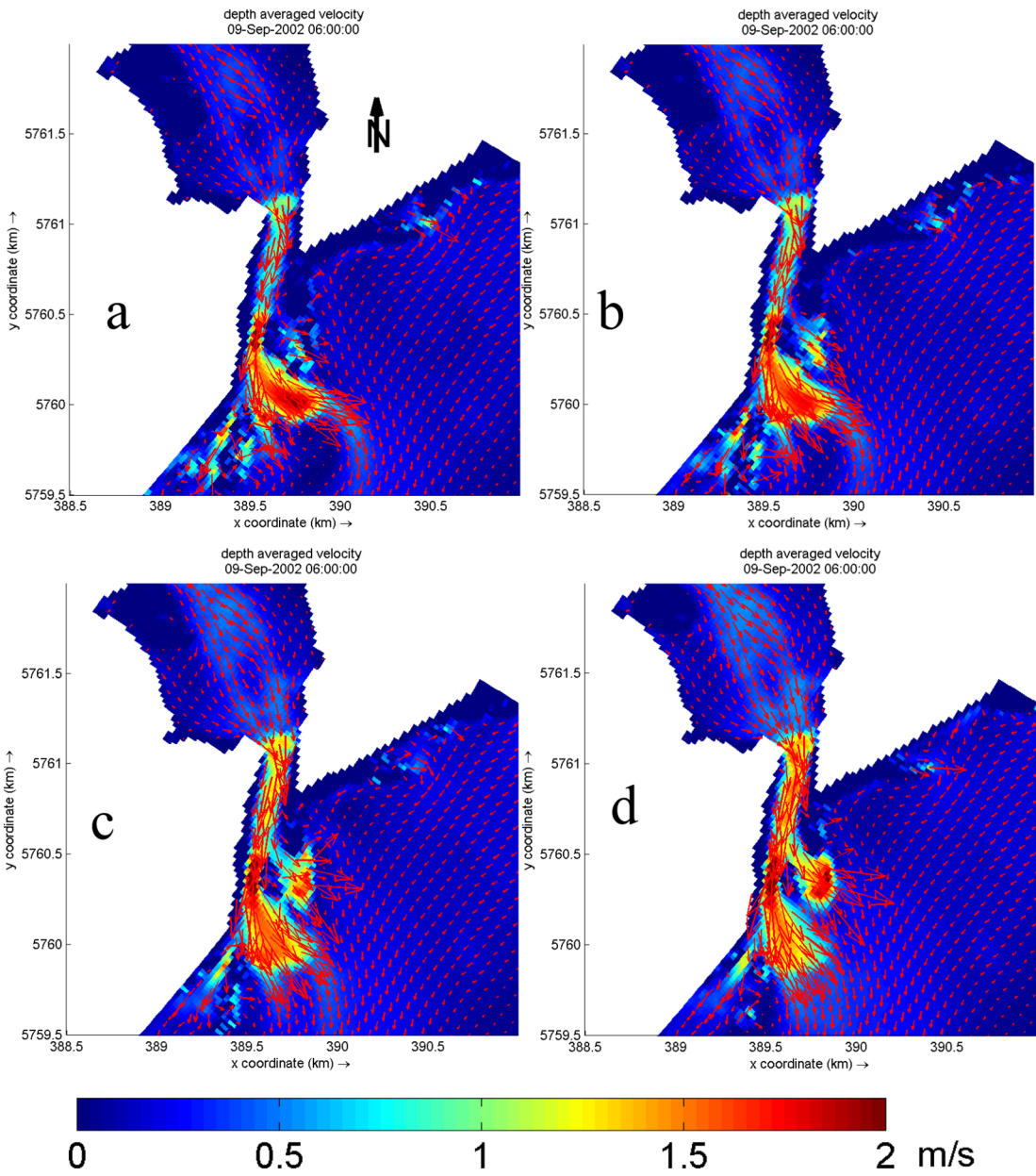


Figure 13

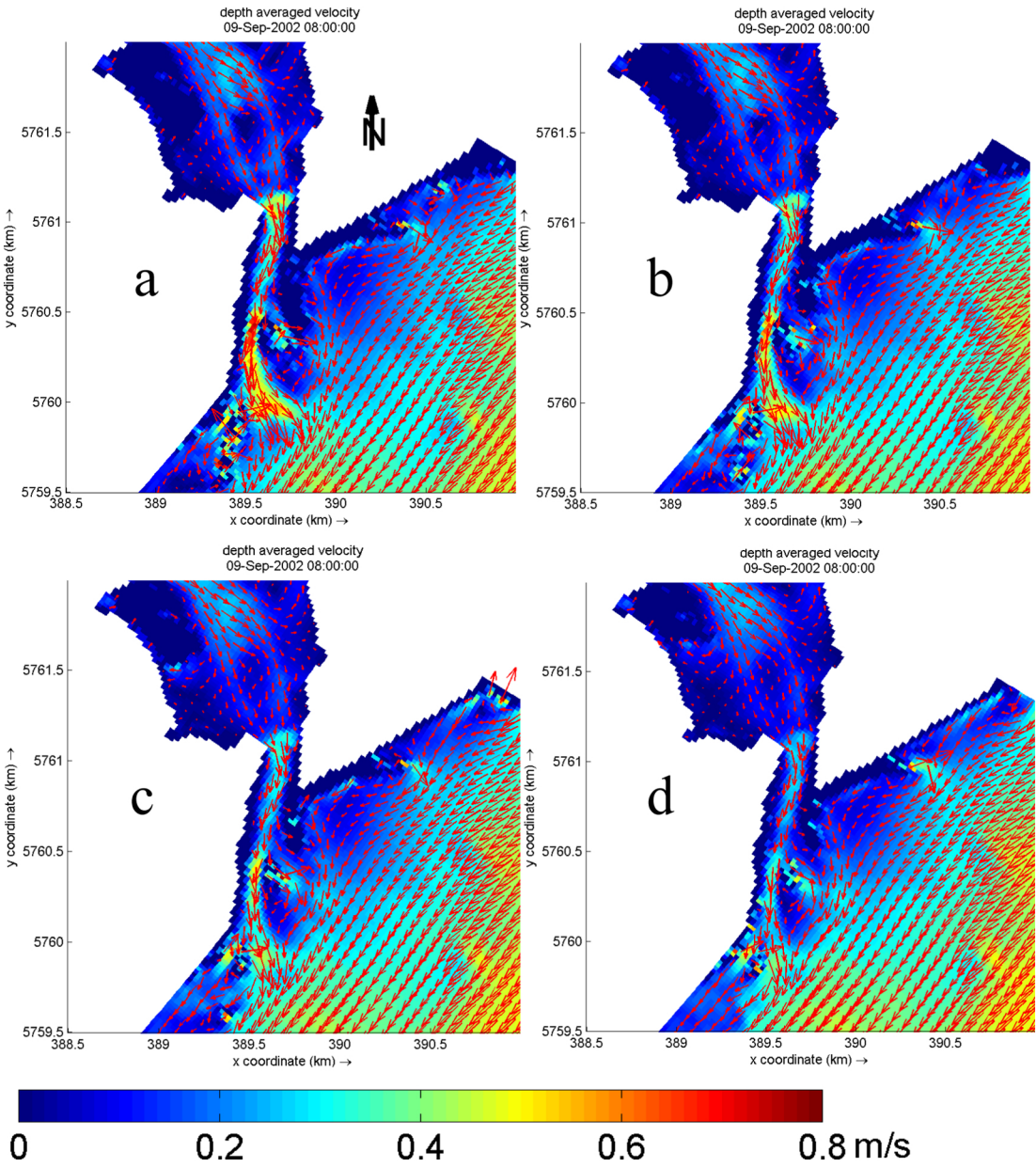


Figure 14

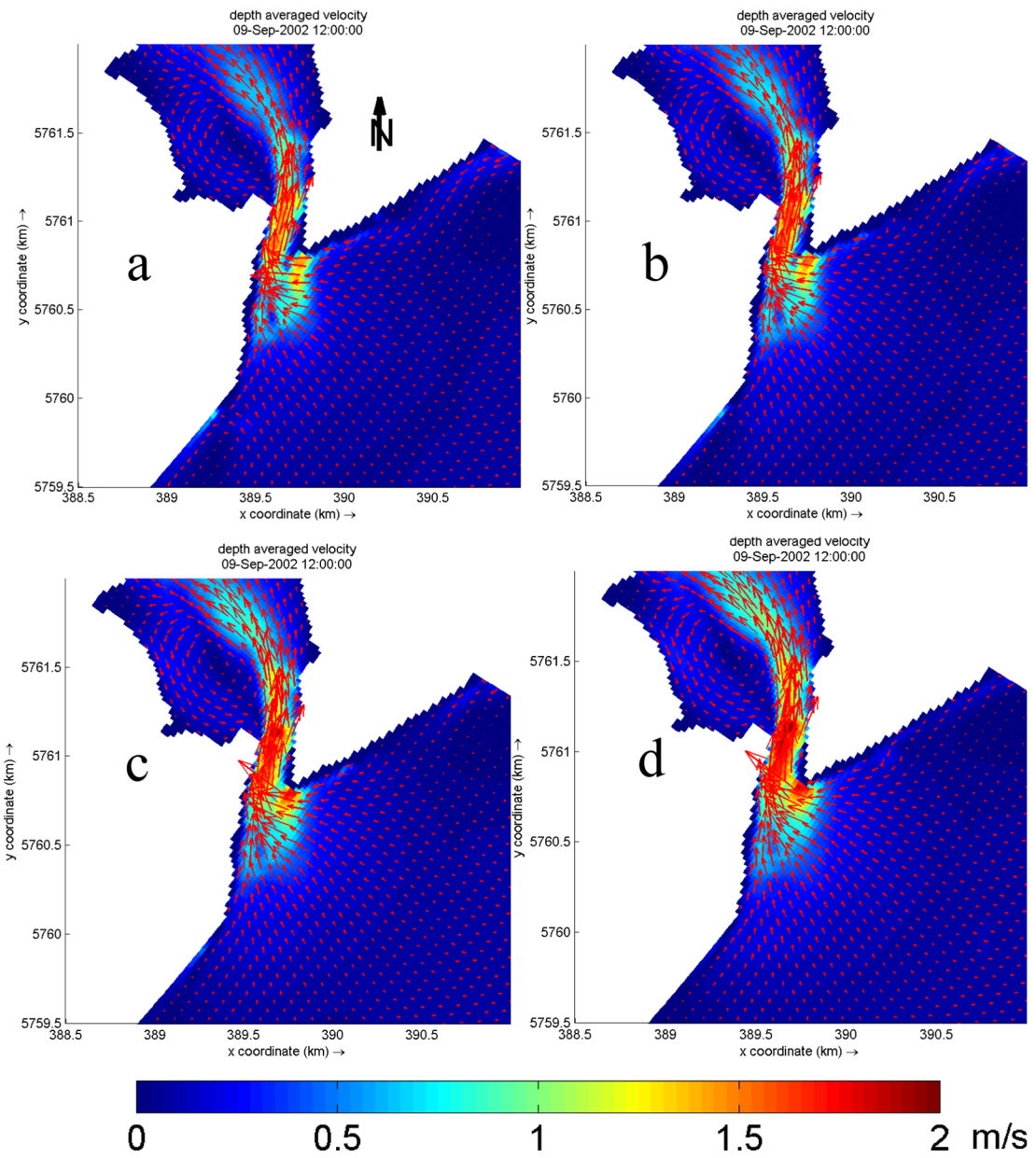


Figure 15

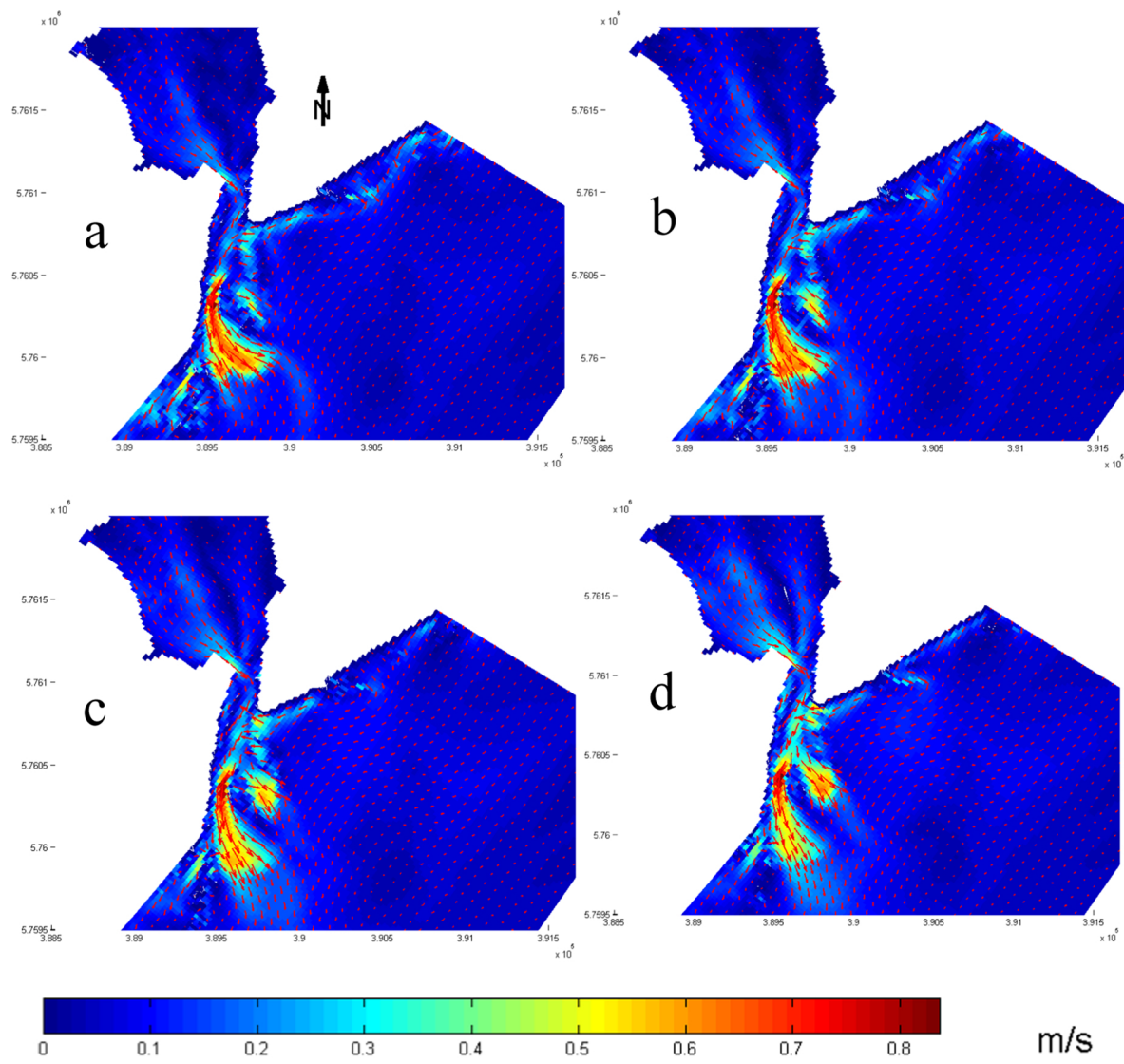


Figure 16

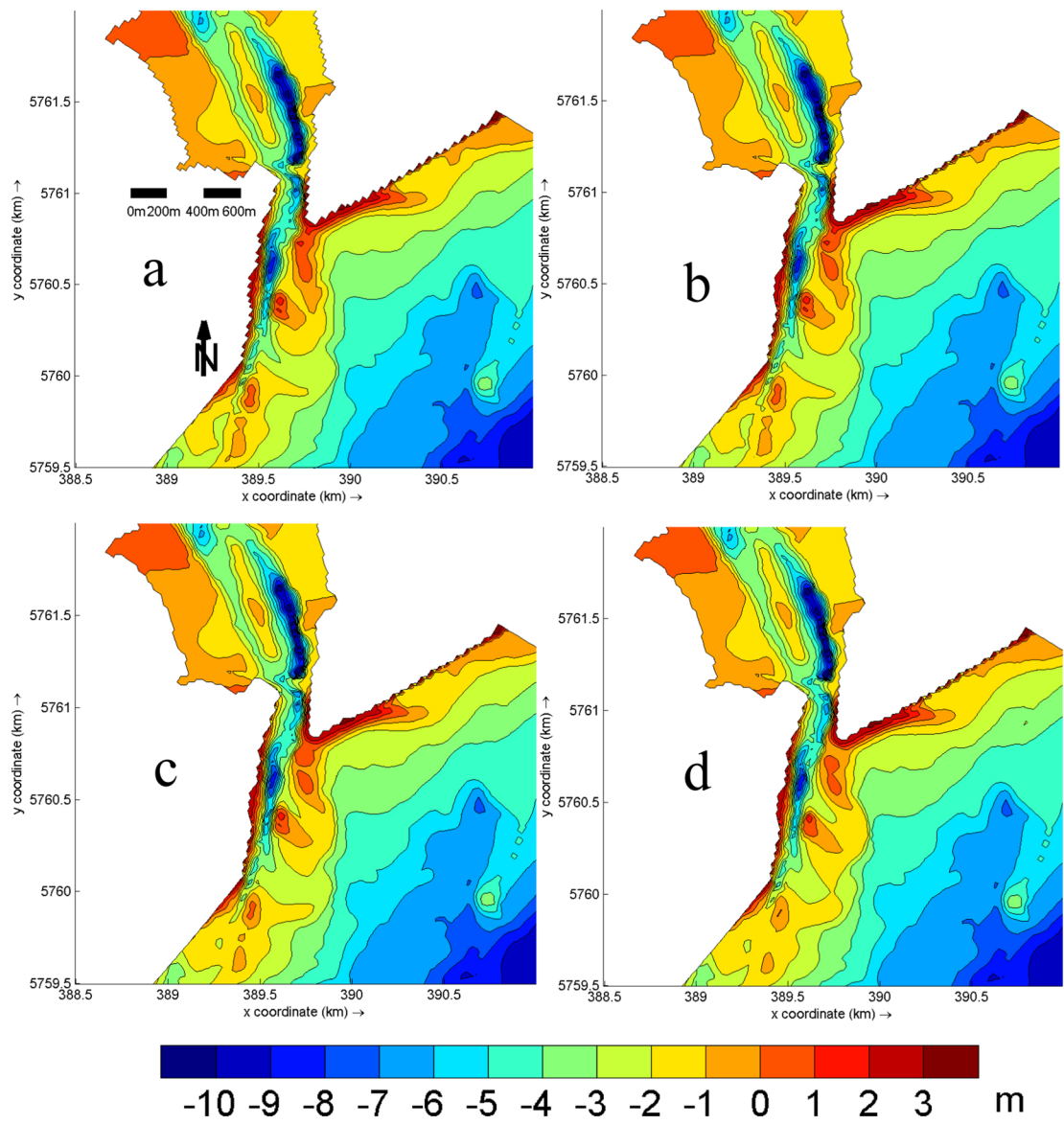


Figure 17

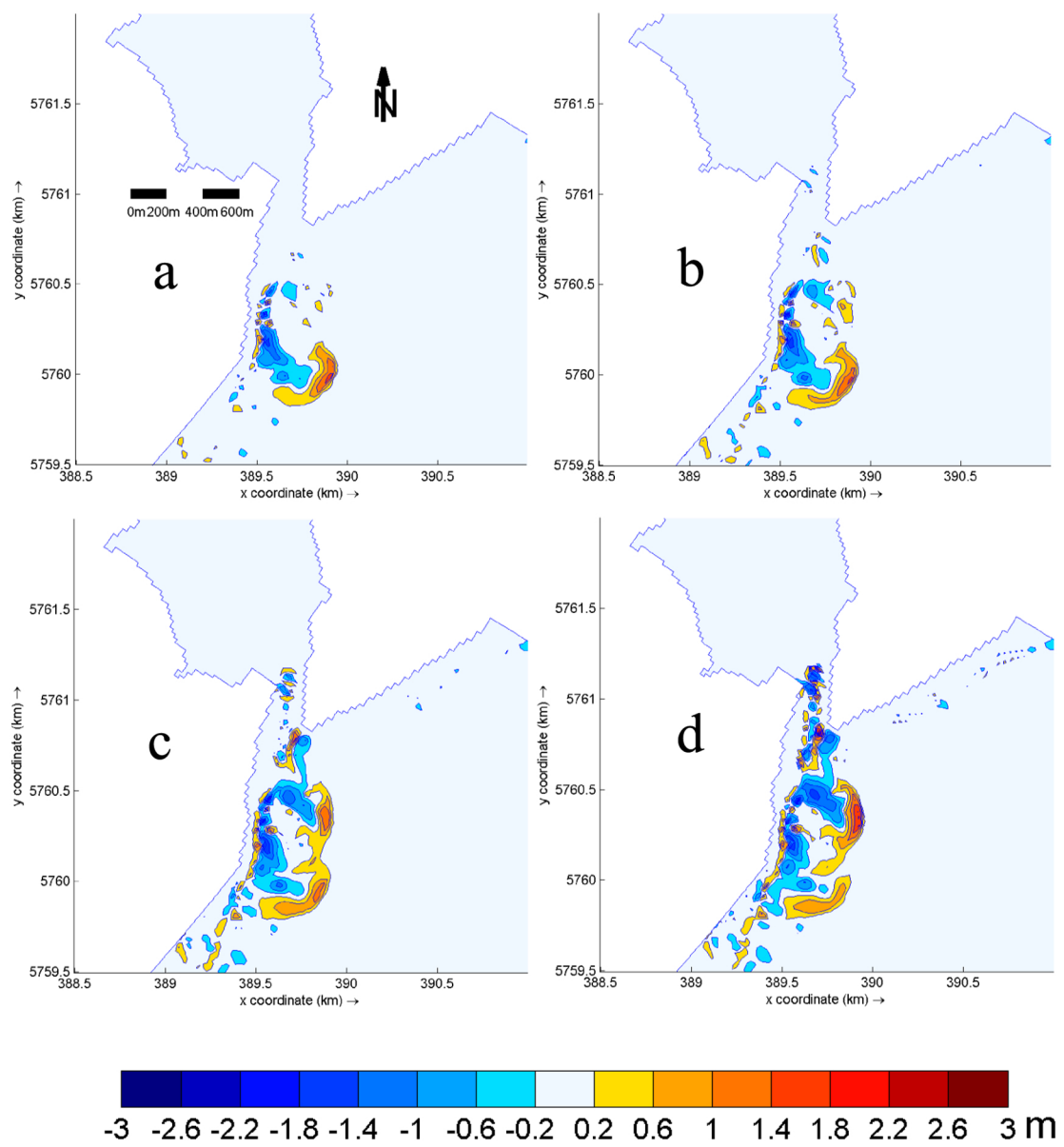


Figure 18

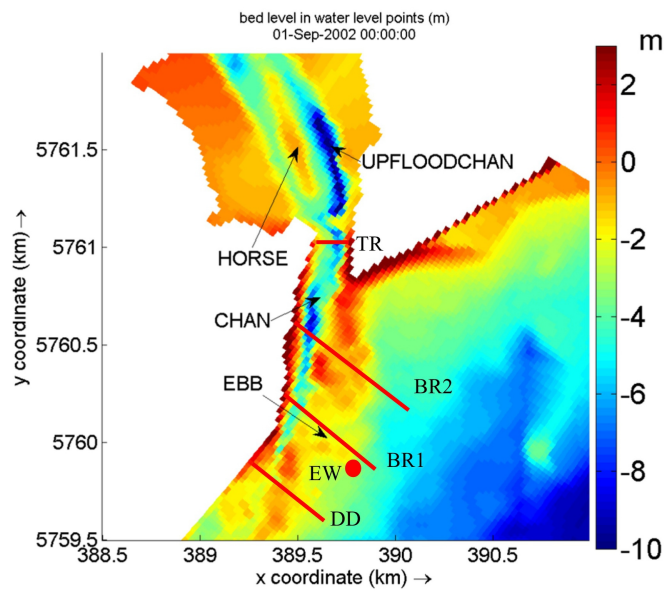


Figure 19

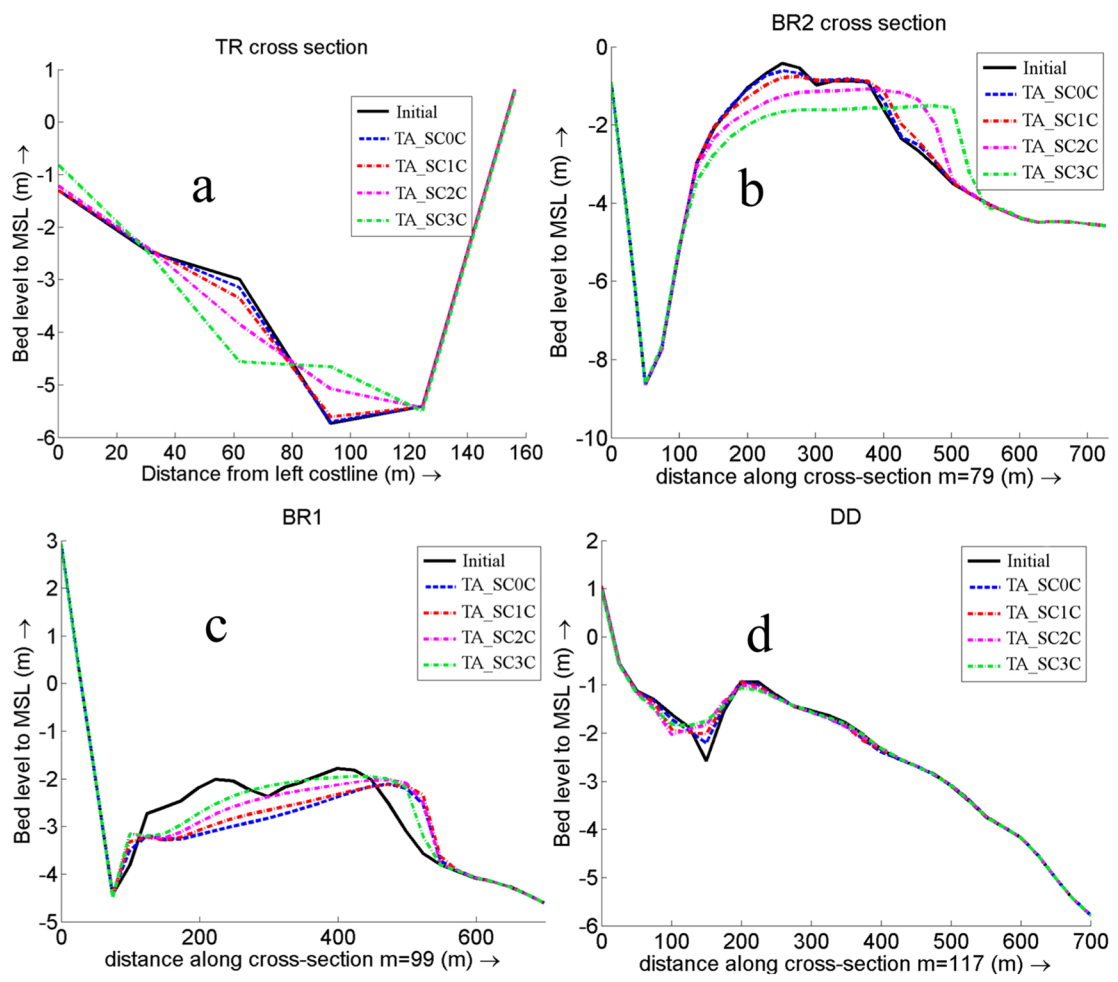


Figure 20

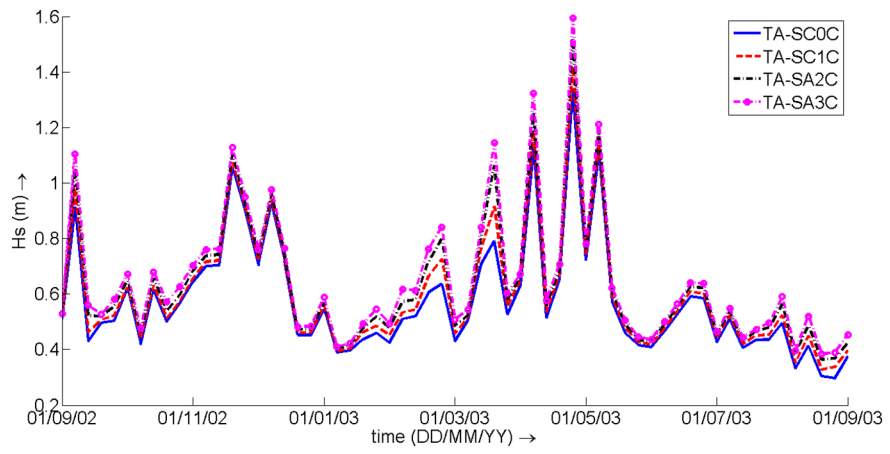


Figure 21

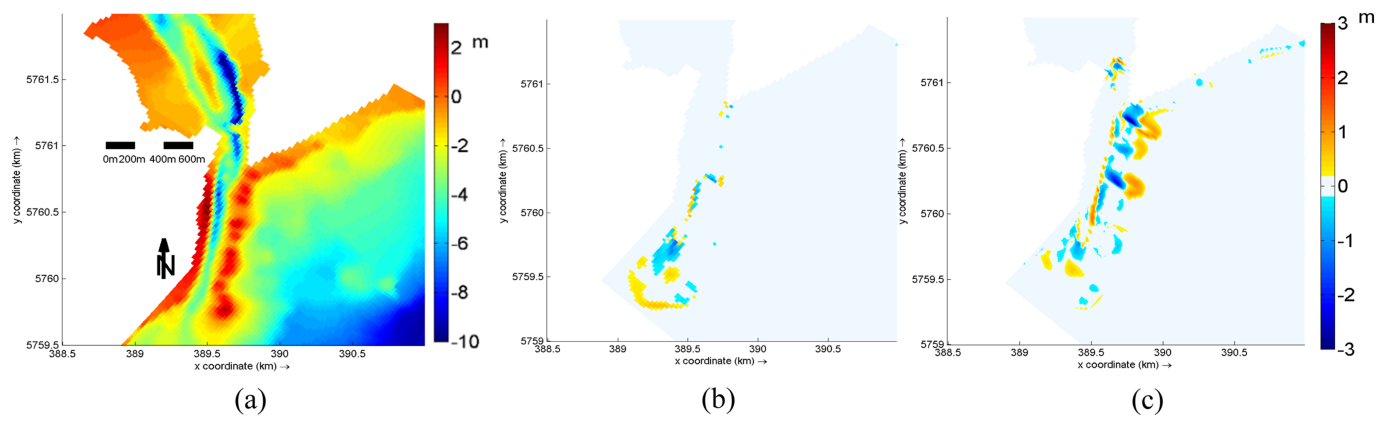


Figure 22

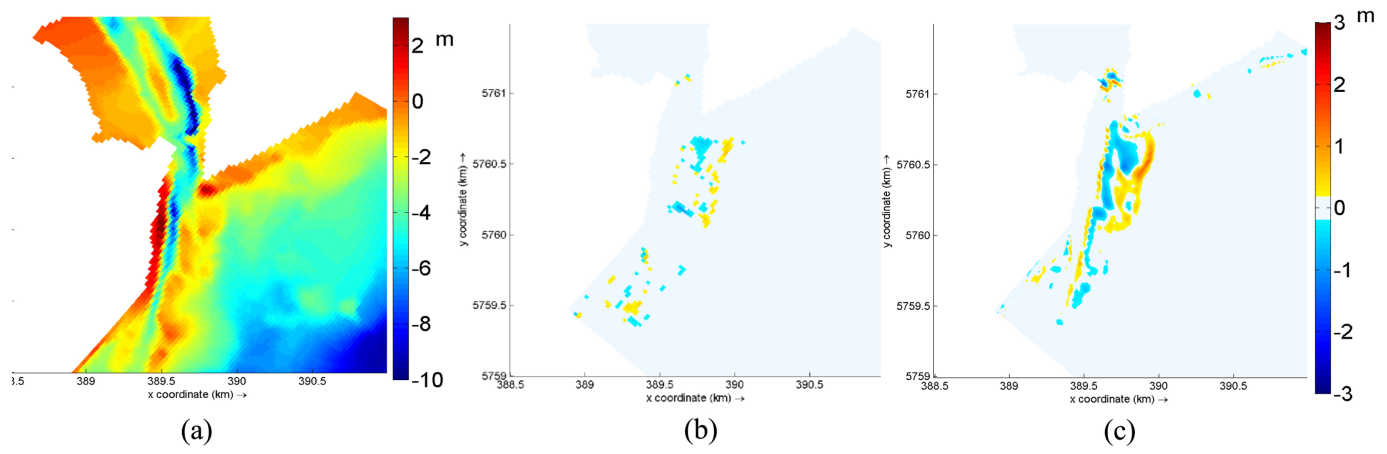


Figure 23